6 Scalar Turbulence within the Canopy Sublayer

Gabriel G. Katul,[1] Daniela Cava,[2] Mario Siqueira,[3] & Davide Poggi[4]

[1]Nicholas School of the Environment, Duke University, United States
[2]Institute of Atmosphere Sciences and Climate, National Research Council, Lecce, Italy
[3]Department of Mechanical Engineering, University of Brasilia, Brazil
[4]Department of Hydraulics, Transport and Civil Infrastructure, Politecnico di Torino, Italy

ABSTRACT

The exchange of scalars between the biosphere and the atmosphere has direct bearing on a large number of problems such as climate change, air and water quality, agricultural management and food security, landscape ecology, and decision making for environmental compliances and policy formulation. Near the canopy-atmosphere interface, turbulent fluctuations in scalar concentrations exhibit complex dynamic behaviour that shows some parallels with the transporting turbulent velocity field. However, the statistical properties of scalar turbulence within and just above the canopy can also be partly decoupled from those of the transporting velocity. Here, a unifying framework is proposed that accounts for vertical variations in scalar sources and sinks within the canopy volume, the lack of equilibrium between production and dissipation terms in second-order scalar budget equations, the rapid changes in turbulent kinetic energy dissipation rate inside canopies, the relative importance of ejections and sweeps, the role of thermal stratification, and the 'near-field' effects of the scalar source on gradient-diffusion theories. Ways in which these same phenomena modify the scalar spectra and scalar-vertical velocity co-spectra within the inertial subrange above the canopy and at scales finer than the wake generation region within the canopy are presented. Finally, the origin of organized eddy structure connected with surface renewal that leads to scalar ramps is briefly discussed. The work draws upon a large number of flume, wind tunnel, and field experiments, and offers novel theoretical scaling arguments as to how coherency in the flow field impacts scalar spectra and scalar-velocity co-spectra at scales smaller than the shear production scales.

6.1 Introduction

Quantifying risks to and benefits from the goods and services offered by the biosphere is moving the study of canopy turbulence from the margins of micrometeorology and agricultural sciences to being a major research thrust in earth system sciences. Scalar transport within canopies remains a vexing research problem confronting basic fluid mechanics, hydrological, atmospheric, ecological, climate, and environmental sciences. The outcomes from scalar transport studies have direct bearing on a large number of disciplines, such as climate change, air and water quality, agricultural management, landscape ecology, and decision making for environmental compliances and policy formulation, to name a few. From the climate-change perspective, concerns about increased anthropogenic CO_2 emissions and the potential role of the biosphere as a carbon sink (Malhi, 2002) resulted in a

Coherent Flow Structures at Earth's Surface, First Edition. Edited by Jeremy G. Venditti, James L. Best, Michael Church and Richard J. Hardy.

proliferation of long-term eddy-covariance flux measurements of carbon dioxide, heat and water vapour across different biomes and climates (Baldocchi *et al.*, 2001). Within the context of this initiative, how to connect biological sources and sinks to monitored turbulent fluxes in the atmosphere remains a problem that can only be approached through fundamental understanding of scalar transport within canopies (Belcher *et al.*, 2012).

However, other equally pressing problems also benefit from studies of scalar transport within the canopy system. Air quality and linkages between atmospheric chemistry and turbulent transport is another major research question in biosphere-atmosphere exchange. This linkage is now receiving significant attention given its implications for food production and ecosystem health (Thomas, 1951). It is now estimated that about 10 to 35% of the world's grain production occurs in regions where ozone pollution can potentially reduce crop yields (Chameides *et al.*, 1994). Ozone uptake by plants or the production and transport of ozone precursors (e.g. isoprene) remains a computationally high-dimensional research problem in which hundreds of chemical reactions governing ozone production and destruction occur at time scales comparable to that of turbulent transport (Gao and Wesely, 1993; Gao *et al.*, 1993; Wolfe and Thornton, 2011). An analogous problem is predicting volatilization of several substances commonly used or produced in agriculture. For example, the application of pesticides to crops and soils is a major source of persistent organic pollutants in the environment. In particular, atmospheric ammonia is recognized as a pollutant for managed ecosystems as its deposition leads to soil acidification and ecosystem eutrophication (Sutton *et al.*, 1993). Both measurement programmes and modelling studies are proposed to track the transport, transformation and deposition of pollutants to water bodies and other terrestrial surfaces. Another area where scalar turbulence is receiving attention is in modelling the micro-climate within large-scale protected agricultural environments (e.g. screen-houses). Water vapour, carbon dioxide, and sensible heat released or taken up by vegetation within such protected environments can substantially alter their immediate turbulent micro-environment, which in turn, affects these fluxes (Manzoni *et al.*, 2011; Siqueira *et al.*, 2012).

Moving up from gas molecules to small sized-particles, the collection of ultra-fine (Lin *et al.*, 2012) and aerosol sized particles (Petroff *et al.*, 2008) by vegetation is another topic receiving significant attention in respiratory human health and in climate research (Pierce and Adams, 2007). For larger particles such as seeds and pollen grains, long-distance dispersal (LDD) by wind is intimately linked to canopy turbulence in ecology (Nathan *et al.*, 2011). Long-distance dispersal has many implications for gene flow, pest control, species expansion, recolonization of disturbed areas, and population dynamics (Nathan *et al.*, 2002). Previous modelling approaches that did not consider the role of turbulence within canopies (especially its coherency) failed to simulate LDD (Nathan *et al.*, 2002), which governs the spatial template over which all other ecological processes (e.g. germination, seedling growth) occur. There is now a clear recognition that seed and pollen escape from the canopy is a necessary condition for LDD and progress in this area must explicitly deal with canopy turbulence (Williams *et al.*, 2006). When all these example problems are taken together, it is clear that a complete theory for scalar transport within canopies must address questions at spatial and temporal scales ranging from millimetres to tens of kilometres and from fractions of seconds to several decades (Katul *et al.*, 2001), well outside the scope of a single chapter.

A number of recent reviews have already covered the canonical structure of turbulence, including scalar turbulence (Shraiman and Siggia, 2000; Warhaft, 2000) in various types of boundary layers (Smits *et al.*, 2011). The mechanical interaction between wind flow and terrestrial plants has also been presented and discussed elsewhere (de Langre, 2008). Moreover, analogies between momentum transport in aquatic and terrestrial vegetation have been recently presented (Katul *et al.*, 2011; Nepf, 2012). Turbulent flows near edges and over hills have also been covered elsewhere (Belcher and Hunt, 1998; Belcher *et al.*, 2012) and these topics are not repeated here. Hence, the compass of this work is the physics of scalar turbulence inside canopies, where the canopy is assumed to be extensive and uniform. Within and immediately above the canopy, a canopy sublayer (hereafter referred to as the CSL) is assumed to extend from the ground surface (or forest floor) up to 2 to 5 times the canopy height h_c (Raupach and Thom, 1981). While the flow statistics are known to be three-dimensional within the CSL (Finnigan, 2000; Finnigan *et al.*, 2009), a single vertical axis (z) describes the flow statistics and canopy properties (e.g. leaf area density) when a proper planar averaging is employed (Wilson and Shaw, 1977; Raupach and Shaw, 1982). In such a flow, the case where a scalar entity is released or absorbed by the canopy elements is treated. The work here focuses on a number of past and novel theories describing the statistical characteristics of scalar concentration fluctuations and turbulent vertical fluxes, as well as their spectral and co-spectral homologues.

6.2 A brief review of scalar turbulence inside canopies

Since the early 1990s, rapid progress has been made in determining the canonical form of the velocity statistics within the CSL, as reviewed elsewhere (Raupach *et al.*, 1996; Finnigan, 2000; Harman and Finnigan, 2007; Finnigan *et al.*, 2009; Belcher *et al.*, 2012). Unlike its atmospheric surface layer counterpart (Katul *et al.*, 2011), the mean velocity profile within the CSL is characterized by an inflection point near $z/h_c \approx 1$, the second moments are inhomogeneous with z inside the canopy, velocity skewness values are large (and opposite in sign for horizontal and vertical velocity components), flatness factors for all the velocity components are far from Gaussian and suggestive of highly intermittent patterns, and second-moment budget equations are not in local equilibrium (a state defined by a balance between the local production and dissipation rates as discussed in Finnigan, 2000). The velocity statistics, when ensemble-averaged to approximate the planar-averaging operation, generally scale with a single canonical length scale that does not vary with z (Raupach *et al.*, 1996).

Quadrant analysis and conditional sampling studies have also revealed that sweeps rather than ejections dominate momentum fluxes for $0.2 < z/h_c < 1.2$ (Finnigan, 2000). Moreover, around $z/h_c = 1$, the bulk flow statistics and instability modes of a plane mixing layer (hereafter referred to as the mixing layer analogy) form a more appropriate model for the canopy flow than those of a boundary layer (Raupach *et al.*, 1996). This finding suggests that dominant large eddies originate from an inviscid instability of the inflected mean velocity profile rather than eddies attached to the canopy top (Raupach *et al.*, 1996). The aerodynamic drag force imposed by the foliage is the primary cause of decreasing (but not suppressing) the mean velocity inside the canopy when compared to the mean velocity aloft, thereby introducing an inflected mean velocity profile. This drag force is also responsible for the so-called 'spectral short cut' mechanism that removes energy from large eddies and directly diverts it to fine scales (Finnigan, 2000) where it is rapidly dissipated, bypassing the so-called classical inertial range eddy-cascade formulated by Kolmogorov's (1941) theory. The total turbulent kinetic energy dissipation rates are generally large inside the canopy and vary nonmonotonically with z as a result of the fine-scale shear layers that develop around the foliage (Poggi *et al.*, 2008; Poggi and Katul, 2009).

Early theoretical work on scalar transport inside canopies assumed that scalar turbulent fluxes are related to their mean concentration gradient (known as K-theory) via a turbulent diffusion coefficient (Raupach and Thom, 1981). Naturally, this theory borrowed from the successes of Monin and Obukhov similarity theory in the atmospheric surface layer (Monin and Obukhov, 1954). Its basic form was and remains the 'work-horse' for inferring scalar turbulent fluxes from mean scalar concentration measurements (Harman and Finnigan, 2008; Bash *et al.*, 2010; Siqueira and Katul, 2010; Wolfe and Thornton, 2011) and much effort has been spent on estimating scalar turbulent diffusivities for different scalars and vegetation cover (Harman and Finnigan, 2008; Bash *et al.*, 2010). However, as early as the mid-1970s, it became clear that assumptions underlying K-theory inside canopies are questionable (Corrsin, 1974). Research in the 1980s identified some of the main limitations, which lead to a number of (interrelated) arguments as to why K-theory fails inside canopies. The three most common ones are (Wilson and Shaw, 1977; Raupach, 1989; Finnigan, 2000):

- variable scalar source distribution within the canopy strongly impacts the apparent diffusivity (near-field effects);
- lack of local balance between turbulent production and dissipation (unlike the atmospheric surface layer);
- vertical transport occurs by (organized) eddy motion whose size is comparable to h_c, which is larger than the scale at which the mean concentration gradients change.

It is no surprise that alternatives to K-theory for scalar transport resulted in: (i) Lagrangian approaches, where the 'near-field' effect of scalar sources was explicitly accounted for, as popularized by the so-called localized near field theory (LNF) described elsewhere (Raupach, 1989; Siqueira *et al.*, 2000), and (ii) higher order Eulerian closure models (Wilson and Shaw, 1977; Meyers and Paw U, 1986; 1987), where the imbalance between production and dissipation terms was explicitly resolved at the expense of transferring the gradient-diffusion argument to higher order mixed moments (Katul and Albertson, 1999). Finally, the role of large-scale coherent motion remained implicit to these two approaches.

6.3 Scope

The compass of this work is to present a unifying framework that bridges all three arguments as to why K-theory fails inside canopies, and further explore the spectral

properties of the main terms causing this failure. This framework accounts for the variations in the scalar sources and sinks, the lack of equilibrium between production and dissipation terms of second-order scalar budgets, the rapid changes in turbulent kinetic energy dissipation rate inside canopies, and the relative importance of ejections and sweeps. How these phenomena modify scalar spectra and scalar-vertical velocity co-spectra within the inertial subrange of the CSL is presented. The work draws upon a large number of flume, wind-tunnel, and field experiments, and offers novel theoretical scaling arguments as to how coherency in the flow impacts scalar spectra and scalar-velocity co-spectra at scales smaller than the shear production scales.

6.4 Scalar turbulence within the CSL

Canopy elements such as foliage, branches and trunks act as sources (or sinks) for scalars that vary appreciably in space. Examples include CO_2 uptake or transpiration by individual leaves via stomatal pores, O_3 uptake on wet or dry leaf surfaces, heat sources or sinks due to radiation interception and emission by canopy elements, and CO_2 respiration from above-ground biomass, among others. Because these scalar sources and sinks are spatially distributed over multiple length scales, double-averaging the constitutive equations becomes necessary (Raupach and Shaw, 1982). This double averaging follows the conventional Reynolds averaging in addition to averaging applied over thin horizontal slabs that include a significant number of canopy elements. Following this double-averaging, the effects of these canopy elements on the flow and scalar field must be modelled, often via a drag force or scalar emission or uptake rate that is often biologically active, as in the case of water vapour, ozone, and CO_2. While the compass of this work is scalar turbulence, it remains necessary to establish a back-ground on the bulk flow field even though the scalar turbulence can be partially decoupled from the velocity (Shraiman and Siggia, 2000).

As a starting point, the mean longitudinal momentum balance for a stationary and planar homogeneous flow at high Reynolds number in the absence of subsidence is considered and is given as

$$\frac{\partial \overline{u}}{\partial t} = 0 = -\frac{\partial \overline{w'u'}}{\partial z} - H_f \frac{\tilde{u}^2}{L_c} \tag{6.1a}$$

(Raupach and Thom, 1981) where w and u are the vertical and longitudinal velocities, overline represents the space and time double-averaging operator, $\overline{u}$ is the mean longitudinal velocity, $\overline{w'u'}$ is the turbulent momentum flux, with primed quantities indicating excursions from their space-time averaged state, respectively, H_f is the Heaviside step function ($H_f = 1$ when $z/h_c \leq 1$ and zero otherwise), L_c is the so-called adjustment length scale (Belcher *et al.*, 2003, 2012) given by $L_c = (C_d a_L)^{-1}$, and C_d is the dimensionless drag coefficient that ranges from 0.1 to 0.3 in terrestrial plants (Katul *et al.*, 2004), a_L is the leaf area density related to the leaf area index (LAI) via $LAI = \int_0^{h_c} a_L(z)dz$. This equation suggests that three dynamically relevant length scales must be accounted for: h_c, L_c, and the eddy size or mixing length over which $\overline{w'u'}$ varies within the canopy (l_m). Geometric constraints on eddy penetration into the canopy require that $l_m < h_c$. Moreover, in vertically uniform canopies, $a_L = LAI/h_c$ so that $L_c/h_c = (C_d LAI)^{-1}$. A mean $C_d = 0.2$ and a dense $LAI = 4\ \mathrm{m^2\ m^{-2}}$ results in $L_c \sim h_c$. Hence, it is common to represent flow statistics inside canopies as a function of only h_c and the friction velocity near the canopy top ($= u_*$). This representation appears to 'collapse' numerous canopy flow experiments (Raupach, 1996; Belcher, Harman and Finnigan, 2012), including artificial canopies composed of rods, strips, crops, and tall forests as shown by others and as further illustrated in Figure 6.1. These normalizing variables for velocity and length are conventionally adopted unless otherwise stated.

6.4.1 The Turbulent flux budget

For a stationary and planar-homogeneous flow in the absence of subsidence and for a high Peclet number, the double-averaged mean continuity and turbulent flux budgets inside the canopy are given as

$$\frac{\partial \overline{T}}{\partial t} = 0 = -\frac{\partial \overline{w'T'}}{\partial z} + H_f S_T$$

$$\frac{\partial \overline{w'T'}}{\partial t} = 0 = -\overbrace{\overline{w'w'}\Gamma_T}^{(T_1)} - \underbrace{\frac{\partial \overline{w'w'T'}}{\partial z}}_{(T_2)} - \overbrace{\frac{1}{\bar{\rho}}\overline{T'\frac{\partial p'}{\partial z}}}^{T_3} + \underbrace{\frac{g}{\overline{T}}\overline{T'T'}}_{T_4} \tag{6.1b}$$

(Siqueira and Katul, 2002) where S_T are heat sources and sinks (used as a prototypical scalar) distributed within the canopy volume, $\overline{w'T'}$ is the turbulent sensible heat flux, $\Gamma_T = \partial\overline{T}/\partial z$, p' is a pressure turbulent perturbation, ρ is the mean air density, g is the gravitational acceleration, and terms T_1, T_2, T_3, and T_4 are the flux production, turbulent transport, scalar-pressure interaction (a de-correlation term), and buoyant production. Here, air

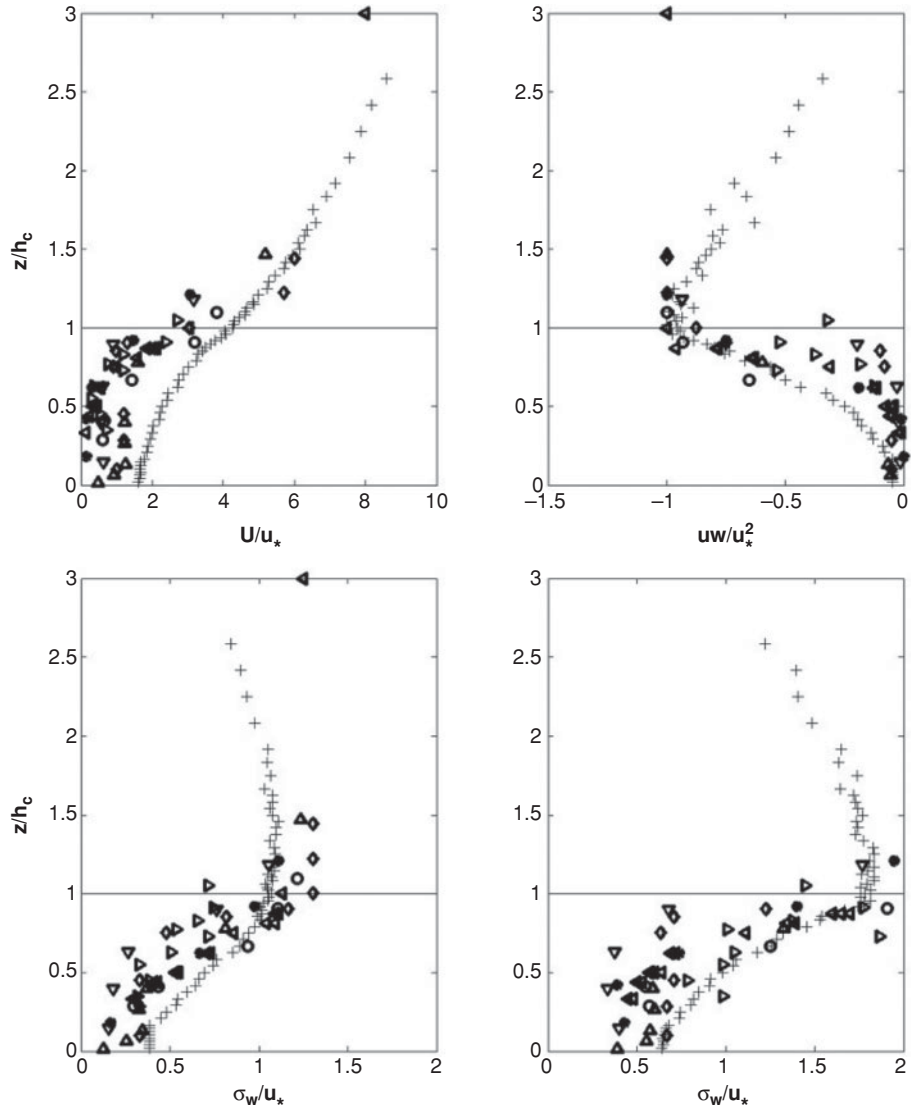

Figure 6.1 Profiles of the first and second moments of the flow field within the CSL normalized by h_c and u_* at the canopy top. These moments include the normalized mean velocity (U), turbulent stress ($\overline{u'w'}$), vertical velocity standard deviation (σ_w), and longitudinal velocity standard deviation (σ_u), collected inside a dense rod canopy in a flume (+), a Loblolly pine plantation (o), and oak hickory hardwood forest (◊), a spruce canopy (∗), a rice canopy (▶), a corn canopy (◀), a Scots pine forest (▲), and an Alpine coniferous forest (▼). Despite the 2 orders of magnitude variations in h_c and u_* across experiments, these two normalizing variables collapse the flow statistics.

temperature is used as a representative scalar for illustration, and much of the formulations here can be revised for other scalars. If a conventional closure model is applied to term T_3, given as

$$\overline{T'\frac{\partial p'}{\partial z}} = C_1\frac{\overline{w'T'}}{\tau} - \frac{1}{3}\frac{g}{\overline{T}}\overline{T'T'} \tag{6.2}$$

(Meyers and Paw U, 1987), then the scalar flux budget can be re-arranged to yield

$$\overline{w'T'} = \frac{\tau}{C_1}\left(-\overline{w'w'}\Gamma_T - \frac{\partial\overline{w'w'T'}}{\partial z} + \frac{4}{3}\frac{g}{\overline{T}}\overline{T'T'}\right) \tag{6.3}$$

(Cava *et al.*, 2006), where τ is a relaxation time scale defined by the ratio of the turbulent kinetic energy (e_{tke}) and its mean dissipation rate (ε_{tke}), and C_1 is a closure constant. This relaxation time scale is a measure of how fast energy-containing eddies dissipate or lose their coherency (or decorrelate in time). Under some conditions, this time scale can also be interpreted as the time scale over which the turbulence comes into a local equilibrium with the surrounding mean velocity gradient (Belcher and Hunt, 1998). Naturally, τ is also a time scale that must be connected to coherent structures, given that these structures significantly contribute to the amount of kinetic energy in the flow. The τ here does not make explicit the precise geometric and topological features defining these coherent structures, but it should capture some of the controls their existence exerts on the closure assumptions. Figure 6.2 shows the variations of e_{tke}, ε_{tke}, and τ collected in a dense rod canopy in a flume. While e_{tke} exhibits a near-monotonic increase with increasing height within the CSL (e.g. $z/h_c \in [0, 2]$), ε_{tke} does not (Figure 6.2). The nonmonotonic nature of ε_{tke} is now supported by a number of flume and wind tunnel experiments (Figure 6.2). This nonmonotonic behaviour for ε_{tke} necessarily leads to nonmonotonic variations in the τ profile within the CSL, which cannot be readily linked to generic time scales such as the integral time scale of the vertical velocity (I_w) or an equilibrium time scale ($\sim k_v z/u_*$) characterizing boundary layers (see Figure 6.2).

Equation (6.3) suggests that any failure of the so-called 'gradient-diffusion' theory (i.e. when $\overline{w'T'} = -\left(\tau\overline{w'w'}/C_1\right)\Gamma_T$, where the turbulent diffusivity is $(\tau\overline{w'w'}/C_1)$) can now be traced back to two terms – the flux-transport and buoyancy terms. Representations similar to this turbulent diffusivity remain popular to date

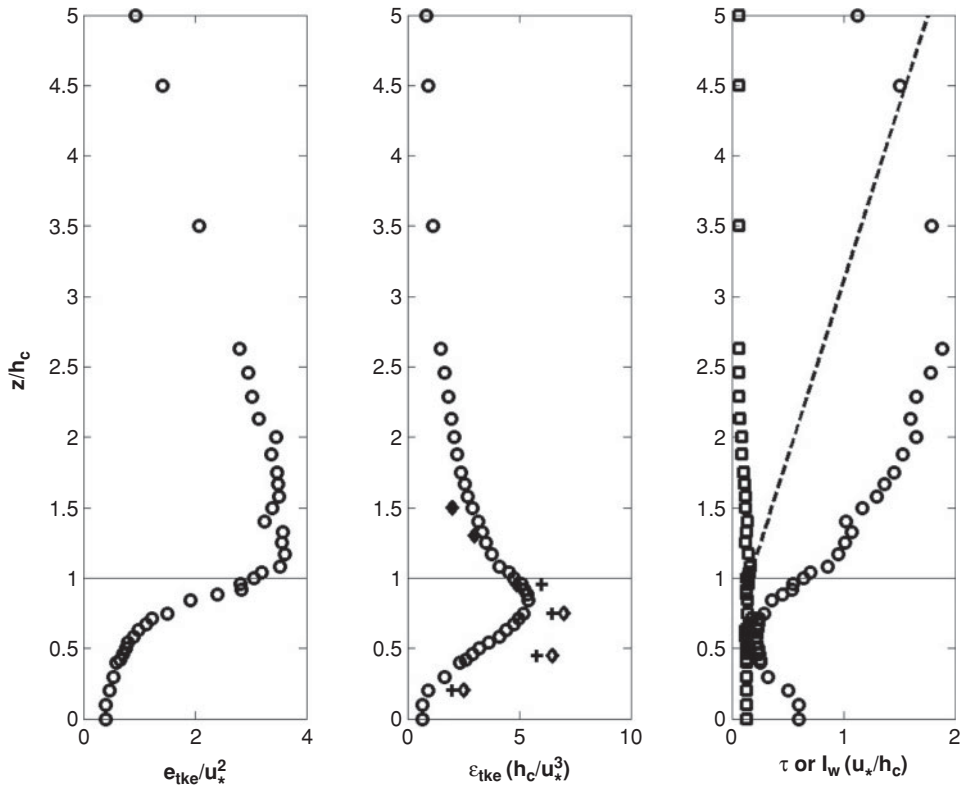

Figure 6.2 Measured variations in the normalized turbulent kinetic energy e_{tke} (left panel) and its mean dissipation rate ε_{tke} (middle panel) as a function of normalized height for the flume experiments. The relaxation (o) and integral (□) time scales are also shown (right panel). All length and velocity scales are normalized by h_c and u_*. The ε_{tke} profiles in the wind tunnel experiments (shown as +, ◊) of Raupach (1988) and the normalized relaxation time scale (dashed line), given by $k_v(z-d)/u_*$, are also shown for reference, where $k_v = 0.4$ is the Von Karman constant. Note the nonmonotonic variations in ε_{tke} and τ with z, especially for $z/h_c \in [0.2, 2.0]$.

within large-scale atmospheric chemistry and transport models (Wolfe and Thornton, 2011) or in scalar transport over complex terrain (Katul *et al.*, 2006c; Katul and Poggi, 2011). The focus here is on the 'global' and 'spectral' role of these two terms inside canopies. The spectral analysis is intended to show the scaling laws describing a range of eddy sizes encoded in τ contribute to both – $\overline{w'T'}$ and $\overline{T'T'}$- at least within a minimalist framework that mirrors the scalar-variance and scalar-flux budgets.

To begin with, two approximations for $\overline{w'w'T'}$ are first treated: one is prognostic and is based on conventional 'local gradient-diffusion' theory, thereby permitting the prediction of turbulent scalar fluxes from their local mean gradients, whereas the other is developed for diagnostic purposes illustrating the close links between $\overline{w'w'T'}$ and the statistical properties of the ejection-sweep cycle, thereby making explicit the complex role of coherent motion on gradient-diffusion closure.

6.4.2 Gradient-diffusion closure for the triple moment

For the most elementary gradient-diffusion approximation that can be applied to $\overline{w'w'T'}$, the flux of the scalar turbulent flux can be related to the mean gradient of the turbulent flux via

$$\overline{w'w'T'} = -C_2 \tau \overline{w'w'} \frac{\partial \overline{w'T'}}{\partial z} \tag{6.4}$$

where C_2 is another similarity constant. Again, this closure approximation can be criticized *ad infinitum*, but the intent here is not to explore its predictive skill, only to account for contributions to $\overline{w'T'}$ originating from $\overline{w'w'T'}$ in the simplest possible manner. Noting that from the mean continuity equation $\partial \overline{w'T'}/\partial z = S_T$, Equation (6.3) can be rewritten as

$$\overline{w'T'} = \frac{\tau}{C_1}\left(-\overline{w'w'}\Gamma_T + C_2 \frac{\partial}{\partial z}\left(\tau \overline{w'w'} S_T\right) + \frac{4}{3}\frac{g}{\overline{T}}\overline{T'T'}\right). \tag{6.5}$$

A number of features now become evident from this derivation. Analogous to the Lagrangian approaches popularized by the so-called localized near-field theory or LNF (Raupach, 1989; Katul *et al.*, 1997; Siqueira *et al.* 2000, 2002, 2003), one source of departure from gradient-diffusion theory applied to the mean scalar gradients is explicitly shown to originate from heat sources and sinks inside the canopy. This effect is analogous to 'near-field' effects in LNF. Moreover, the expression above does not require a locally homogeneous flow field as assumed in LNF because the vertical gradients in $\overline{w'w'}$ are explicitly considered. When expanding

$$\frac{\partial}{\partial z}\left(\tau \overline{w'w'} S_T\right) = \tau \overline{w'w'} \frac{\partial S_T}{\partial z} + S_T \frac{\partial}{\partial z}\left(\tau \overline{w'w'}\right) \tag{6.6}$$

and noting that when

$$\left| \frac{\frac{\partial}{\partial z}\left(\tau \overline{w'w'}\right)}{\tau \overline{w'w'}} \right| \ll \left| \frac{\frac{\partial S_T}{\partial z}}{S_T} \right| \tag{6.7}$$

a locally homogeneous flow (as in LNF) becomes a plausible approximation – at least within the confines of the gradient-diffusion closure adopted for $\overline{w'w'T'}$. Another feature evident from this derivation, which could not have been readily predicted from LNF, is the explicit role of thermal stratification in the failure of gradient-diffusion theory for heat inside canopies. The T_4 term here is always positive for heat (but not necessarily for other scalars) and can be large during daytime conditions, especially when some mild nonstationarity contributes to the measured turbulent temperature variance.

Finally, equation (6.1b) can be rewritten as

$$\frac{\partial^2 \overline{w'T'}}{\partial z^2} + \frac{\frac{\partial}{\partial z}\left(\tau \overline{w'w'}\right)}{\tau \overline{w'w'}} \frac{\partial \overline{w'T'}}{\partial z} + \frac{C_1}{C_2 \tau^2 \overline{w'w'}} \overline{w'T'} = \frac{1}{C_2 \tau}\Gamma_T + \frac{1}{C_2 \tau \overline{w'w'}} \frac{4}{3}\frac{g}{\overline{T}}\overline{T'T'} \tag{6.8}$$

(Cava *et al.* 2006), which shows that the flux profile $\overline{w'T'}(z)$ can be interpreted as a solution to a second-order ODE formed as a superposition of two solutions. The first is a homogeneous solution to Equation (6.8) obtained by setting the right-hand to zero and hence entirely described by vertical variations in τ (that is connected to the coherency in the flow) and $\overline{w'w'}$. The second solution is needed to match the nonhomogeneous term (i.e. the right hand) in which the vertical variations in the mean scalar quantities ($\overline{T}$) and their variance ($\overline{T'T'}$) further adjust and modify the shape of $\overline{w'T'}(z)$. To summarize, the above ODE describing $\overline{w'T'}(z)$ shows that a local gradient-diffusion argument applied to the flux-transport term can recover all the desirable features in Lagrangian models (such as LNF), and goes further by revealing the explicit effects of thermal stratification within the canopy via $\overline{T'T'}$ (discussed later). Next, a nonlocal description to $\overline{w'w'T'}$, connected to the ejection-sweep cycle, is explored.

6.4.3 Linking the triple moment to the ejection-sweep cycle

Ejections and sweeps are commonly defined and identified via quadrant analysis (Lu and Willmarth, 1973; Antonia, 1981). Quadrant analysis refers to a joint scatter plot across four quadrants in a Cartesian plane whose abscissa is an arbitrary flow variable s' (e.g. $s' = u'$, T') and whose ordinate is generally the vertical velocity w'. For flow variables where $\overline{w's'} < 0$, such as momentum ($s' = u'$), used here for illustrating the terminology and definitions, the four quadrants indicate four possible modes of transfer: events in quadrants II ($u' < 0$, $w' > 0$) and IV ($u' > 0$ and $w' < 0$) are ejections and sweeps respectively, whereas events in quadrants I ($u' > 0$ and $w' > 0$) and III ($u' < 0$ and $w' < 0$) are outward and inward interactions, respectively (Antonia, 1981). Opposite quadrants define scalar fluxes for the flow variables where $\overline{w's'} > 0$, such as daytime air temperature ($s' = T'$). The imbalance in contributions to momentum (or scalar) transfer originating from sweeps and ejections can be defined using the difference in turbulent stress (or scalar flux) fraction contributions of quadrant IV and quadrant II (for $\overline{w'u'} < 0$) as

$$\Delta S_o = \frac{\overline{u'w'}_{IV} - \overline{u'w'}_{II}}{\overline{u'w'}} \tag{6.9}$$

(Nakagawa and Nezu, 1977; Raupach, 1981), where $\overline{u'w'}$ is the total momentum flux (assumed negative) and $\frac{\overline{u'w'}_{IV}}{\overline{u'w'}}$ and $\frac{\overline{u'w'}_{II}}{\overline{u'w'}}$ are the stress fractions in quadrant IV and II, respectively. This definition ensures that ΔS_o is bounded between –1 and 1 (assuming $|\overline{u'w'}| > 0$). Based on this definition, sweeps (or ejections) dominate the momentum transfer when $\Delta S_o > 0$ (or $\Delta S_o < 0$). The quantity ΔS_o becomes ill defined when the mean stress or turbulent flux become small ($|\overline{u'w'}|$ or $|\overline{w'T'}| \to 0$). A number of experiments have shown that ΔS_o varies appreciably with z and canopy density (see Figure 6.3) especially for $z/h_c < 2$.

Using the Gram–Charlier cumulant expansion method (or CEM) for the joint probability density function (or JPDF) described elsewhere (Frenkiel and Klebanoff, 1967) truncated to third order, it was demonstrated (Raupach, 1981) that:

$$\Delta S_o = \frac{1 + R_{uw}}{R_{uw}\sqrt{2\pi}}\left[\frac{2C_A}{(1+R_{uw})^2} + \frac{C_B}{1+R_{uw}}\right] \tag{6.10}$$

where

$$C_A = (1+R_{uw})\left[\frac{1}{6}(M_{03} - M_{30}) + \frac{1}{2}(M_{21} - M_{12})\right]$$
$$C_B = -\left[\frac{1}{6}(2 - R_{uw})(M_{03} - M_{30}) + \frac{1}{2}(M_{21} - M_{12})\right] \tag{6.11}$$

and $R_{uw} = \frac{\overline{u'w'}}{\sigma_u\sigma_w}$, $M_{ij} = \frac{\overline{u'^i w'^j}}{\sigma_u^i \sigma_w^j}$, $\sigma_s = \sqrt{\overline{s'^2}}$ and where $u'^j|_{j=2} \to u'^2$. A number of studies noted that contributions to ΔS_o originating from the term $\frac{1}{6}(M_{03} - M_{30})$ are small when compared to $\frac{1}{2}(M_{21} - M_{12})$. Hence, this observation led them to propose a simplified expression for ΔS_o, which they labelled as an incomplete third-order CEM (or ICEM) given as:

$$\Delta S_o \approx \frac{1}{2R_{uw}\sqrt{2\pi}} M_{21} - M_{12} \tag{6.12}$$

where

$$M_{21} = \frac{\overline{u'u'w'}}{\sigma_u^2\sigma_w}$$
$$M_{12} = \frac{\overline{u'w'w'}}{\sigma_u\sigma_w^2}. \tag{6.13}$$

For heat transport with $\overline{w'T'} < 0$, the derivation and nomenclature remains the same as for momentum. However, when $\overline{w'T'} > 0$, the imbalance in contribution of sweeps and ejection is evaluated by using the difference in heat flux fraction originating from quadrants III and I. Moreover, the application of the CEM and ICEM formulations requires a minor coordinate transformation as discussed elsewhere, when $\overline{w'T'} > 0$. When the JPDF is Gaussian, $\Delta S_o = 0$. Stated differently, asymmetry in the JPDF is necessary for sweeps and ejections to contribute differently to turbulent fluxes. The fact that $\Delta S_o \neq 0$ and can vary with z (Raupach, 1981; Poggi *et al.*, 2004; Katul *et al.*, 2006a) has important implications to gradient-diffusion closure models (see Figure 6.3 as an example for momentum). To illustrate, assuming a linear relation between M_{12} and M_{21} as shown in many wind tunnel and flume experiments and for dense canopies (Cava *et al.*, 2006), the flux-transport term responsible for perturbing gradient-diffusion theory can now be linked to ΔS_o using ICEM to yield

$$M_{12} = \frac{\overline{T'w'w'}}{\sigma_T\sigma_w^2} \approx \frac{2\sqrt{2\pi}R_{wc}}{\gamma}\Delta S_0 \tag{6.14}$$

where γ is a proportionality constant linking M_{12} and M_{21}. Hence, for near-neutral conditions (e.g. $g \approx 0$), ejections and sweeps perturb gradient diffusion theory via an additive term given as

$$\overline{w'T'} = -\underbrace{\frac{\tau\sigma_w^2}{C_1}\frac{\partial\overline{T}}{\partial z}}_{\substack{\text{Gradient}-\\ \text{Diffusion}}} - \underbrace{\frac{\tau}{C_1}\frac{\partial}{\partial z}\left(\frac{2\sqrt{2\pi\overline{w'w'}}\sigma_T R_{wc}}{\gamma}\Delta S_o\right)}_{\substack{\text{Perturbation to gradient}-\text{diffusion}\\ \text{due to ejections and sweeps}}}. \tag{6.15}$$

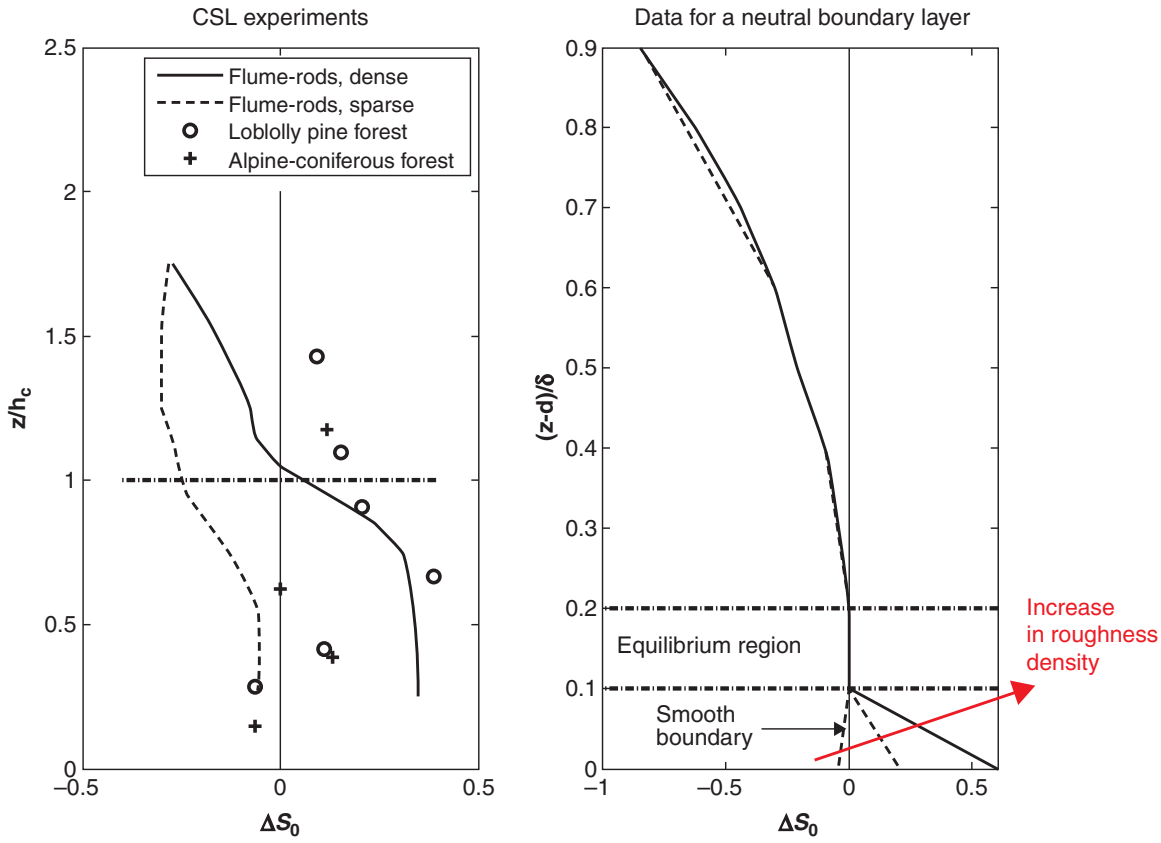

Figure 6.3 Left: Variations of measured ΔS_o for momentum with normalized height for a dense (solid) and a sparse (dashed) rod canopy. Measured values for a pine forest (Katul and Albertson, 1998) and an alpine coniferous forest (Cava *et al.*, 2006) are also shown – all suggesting that sweeps dominate momentum transport in dense canopies. Right: Variations of measured ΔS_o across the entire boundary layer above rough and smooth surfaces in a wind tunnel (three sample data sets taken from Raupach (1981) for smooth, intermediate roughness, and very rough). The normalizing variables here are h_c for the canopy experiments and the boundary-layer thickness δ for the wind-tunnel experiments. A positive ΔS_o indicates that the momentum flux is dominated by sweeps. Note that within the surface layer, where $(z-d)/\delta \in [0.1, 0.2]$, $|\Delta S_o|$ and $\partial \Delta S_o/\partial z$ are small. Near the canopy top however, both $|\Delta S_o|$ and $\partial \Delta S_o/\partial z$ are large.

Given that the ΔS_o profile is generally not known, Equation (6.15) should only be viewed as 'diagnostic' rather than prognostic. It is intended to show how variations from the surface layer into the CSL across various stability conditions, which introduce a vertical gradient in ΔS_o, bias flux predictions using gradient-diffusion theory.

6.4.4 Scalar variance

The previous section demonstrated how ejections and sweeps perturb gradient-diffusion theories; this section focuses on the role of the scalar variance term $(= 4/3)(g/\bar{T})\overline{T'T'}$ by examining the processes and scales impacting its production and dissipation. The air temperature variance budget for a stationary and planar homogeneous flow in the absence of subsidence (Garratt, 1992; Siqueira and Katul, 2002) is

$$\frac{\partial \overline{T'T'}}{\partial t} = 0 = -2\overbrace{\overline{w'T'}\Gamma_T}^{(T_1)} - \underbrace{\frac{\partial \overline{w'T'T'}}{\partial z}}_{(T_2)} - 2\overbrace{\varepsilon_{TT}}^{(T_3)} \qquad (6.16)$$

where T_1, T_2, and T_3 are associated with the variance production, turbulent transport, and variance dissipation (as before). By again invoking conventional closure approximations for the variance dissipation and its transport terms (Siqueira and Katul, 2002), given as

$$\varepsilon_{TT} = C_3 \frac{\overline{T'^2}}{\tau}, \quad \overline{w'T'T'} = \frac{\tau}{C_4}\left[-\overline{w'^2}\frac{\partial \overline{T'^2}}{\partial z}\right] \qquad (6.17)$$

where C_3 and C_4 are closure constants, the variance budget reduces to

$$\frac{\partial \overline{T'T'}}{\partial t} = 0 = -2\overline{w'T'}\Gamma_T - \frac{\partial}{\partial z}\left[-\frac{\tau}{C_4}\overline{w'^2}\frac{\partial \overline{T'^2}}{\partial z}\right] - 2C_3\frac{\overline{T'^2}}{\tau}. \quad (6.18)$$

This equation can be rearranged to yield:

$$\frac{\partial^2 \overline{T'^2}}{\partial z^2} + \frac{\frac{\partial}{\partial z}\left[\tau\overline{w'^2}\right]}{\tau\overline{w'^2}}\frac{\partial \overline{T'^2}}{\partial z} - \frac{2C_3C_4}{\overline{w'^2}\tau^2}\overline{T'^2} = \frac{2C_4\overline{w'T'}}{\overline{w'^2}\tau}\Gamma_T. \quad (6.19)$$

Equations (6.18) and (6.19) must be solved simultaneously when Γ_T, $\overline{w'^2}$, and $\tau(z)$ are known.

Comparison between measured and modelled sensible heat fluxes inside a Loblolly pine canopy and an alpine canopy are shown in Figures 6.4a to 6.4c. In this comparison, Γ_T was directly inferred from measurements and $\overline{w'^2}$ and τ were computed using a higher order closure schemes for the flow field. Clearly, accounting for $\frac{g}{T}\overline{T'T'}$ improves the model prediction over the near-neutral case ($g = 0$). Moreover, the agreement between measured and modelled ΔS_o in Figure 6.4b is rather encouraging. $\overline{T'T'}$ contributes to flux predictions, so its spectral properties are considered next, especially inside canopies.

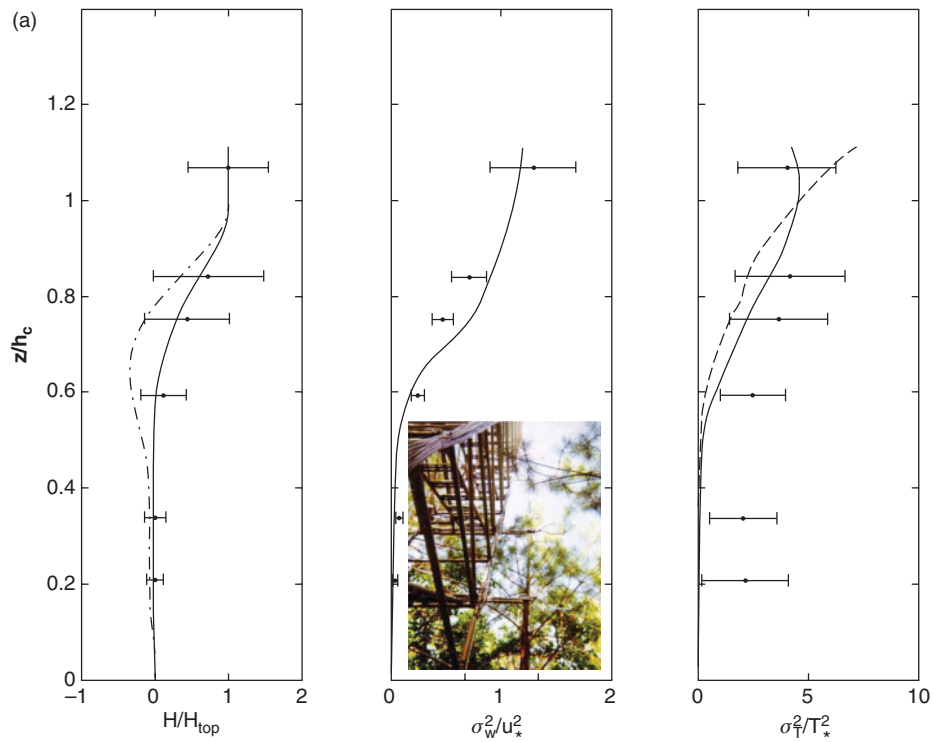

Figure 6.4 (a) Comparison between measured (symbols) and modelled (lines) sensible heat flux $H_s(z) = \rho C_p \overline{w'T'}(z)$ profiles within a southern Loblolly pine forest for neutral ($g = 0$, dashed line) and unstable conditions normalized by their values above the canopy (left panel). The model calculations are driven by measured $\Gamma_T(z)$. The velocity field, including $\sigma_w(z)$, and the relaxation timescale needed in the flux budget equations were computed using a higher order closure model described elsewhere (Siqueira and Katul, 2002). For reference, the $\sigma_w(z)$ comparison is shown (middle panel) for the pine forest (see picture). The modelled σ_T^2 from the scalar variance budget is also used in the thermal stratification term of the sensible heat flux budget and its normalized value is compared to measurements as well (right panel). The normalizing variable for σ_T is $T_* = \overline{w'T'}/u_*$ at the canopy top. (b) Measured profiles of σ_w, $\overline{T}$, σ_T (top panels) in an alpine coniferous forest and comparison between measured and modelled sensible heat flux (bottom – left), triple moments (bottom – middle), and ΔS_o (bottom – right). Three modelled sensible heat flux profiles are shown: (i) K-theory (dotted line) with only measured Γ_T, σ_w, and modelled τ used, the heat-flux budget in the absence of thermal stratification (dashed), and the full sensible heat flux budget (i.e. including measured σ_T); the modelled $\overline{w'w'T'}$ is based on gradient-diffusion closure (Equation (6.4)), and the modelled ΔS_o is based on the ICEM expansion and modelled $\overline{w'w'T'}$ (Equation (6.14)). These comparisons are for unstable atmospheric conditions (defined at the canopy top). (c) Same as Figure 4b but for stable conditions at the canopy top.

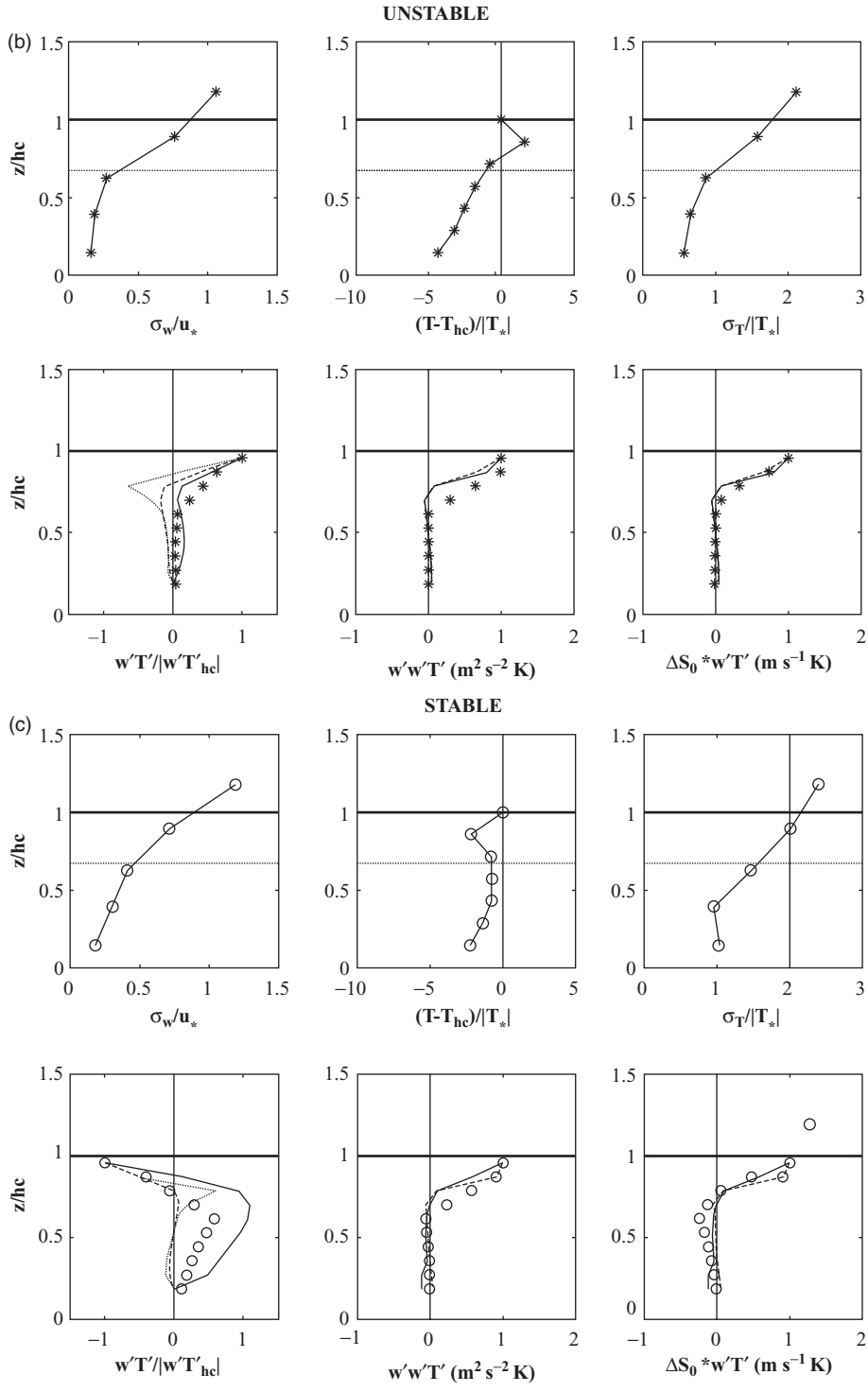

Figure 6.4 (*Continued*)

6.4.5 Scalar spectra

For exploring scales controlling aspects of the scalar variance (and its decay) inside a canopy, the concentration fluctuation spectra $\phi_{cc}(k)$ of a generic scalar c (including temperature) is considered, where $\int_0^\infty \phi_{cc}(k)dk = \overline{c'c'}$ and k is the wavenumber. The focus of this section is not on all aspects of $\phi_{cc}(k)$ but rather on the role of wake generation in modifying the scaling laws of $\phi_{cc}(k)$. It is precisely the role of these wake-generation mechanisms on $\phi_{cc}(k)$ that have not been well studied in canopy turbulence.

As a starting point for exploring $\phi_{cc}(k)$ at these scales, the case for locally homogeneous and isotropic turbulence is treated in the absence of a strong source or production term so that $\Gamma_T \approx 0$), and for $kh_c \gg 1$, resulting in an equation given by

$$\frac{\partial \phi_{cc}(t,\, k)}{\partial t} = \left(W_c(t,\, k) - 2k^2 \chi_c \phi_{cc}(t,\, k)\right) \quad (6.20)$$

(Corssin, 1964; Poggi, Katul and Albertson, 2006; Danaila and Antonia 2009) where $W_c = -\partial T_{r,c}/\partial k$ is the transfer of scalar variance via interactions between turbulent velocity and scalar concentration fluctuations, which is analogous to the flux transfer term in the scalar variance budget (Equation 6.16), and the term $2k^2\chi_c\phi_{cc}(t,\, k)$ represents the molecular dissipation (analogous to ε_{TT}), where χ_c is the molecular diffusivity of scalar c. Assuming that the term $T_{r,c}$ responsible for transferring variance from wavenumbers smaller than k to wavenumbers larger than k is modelled in direct proportion to the available scalar energy at k, which is given as $k\phi_{cc}(k)$, via a 'scale-dependent' relaxation time scale $\tau(k)$, then $T_{r,c} = k\phi_{cc}(k)/\tau(k)$ and the scalar spectral budget equation at steady-state reduces to

$$0 = \frac{\partial}{\partial k}\left(\frac{k\phi_{cc}(k)}{\tau(k)}\right) - 2k^2\chi_c\phi_{cc}(k). \quad (6.21)$$

The general solution for an arbitrary $\tau(k)$ can be expressed as

$$\phi_{cc}(k) = A_1 \exp\left[-\int \frac{\tau(k)}{k}\frac{\partial}{\partial k}\left(\frac{k}{\tau(k)}\right) + 2\chi_c k\tau(k)\right] \quad (6.22)$$

(Danaila and Antonia, 2009) where A_1 is an integration constant.

One possible generalization of the definition of τ to a wave-number dependent time scale is given as

$$\tau(k) = \left(\int_0^k p^2\phi_{TKE}(p)dp\right)^{-1/2} \quad (6.23)$$

(Poggi, Katul and Vidakovic, 2011), where ϕ_{TKE} is the kinetic energy spectrum. This representation for $\tau(k)$ assumes that turbulent eddies at wavenumber k are strained by all larger eddies characterized by wavenumbers $< k$. For a power-law TKE spectrum given by $\phi_{TKE} = A_{TKE}k^{-m}$, this relaxation time scale becomes a power-law given by $\tau(k) = \left[(3-m)/(A_{TKE}k^{3-m})\right]^{1/2}$ (for $m < 3$), and the scalar spectrum, subject to the condition that the variance dissipation rate is $\varepsilon_{cc} = \chi_c \int_0^\infty p^2\phi_{cc}(p)dp$, becomes

$$\phi_{cc}(k) = \frac{\varepsilon_{cc}(3-m)^{1/2}}{2\sqrt{A_{TKE}}}\left(k^{(m-5)/2}\right) \exp\left[-\frac{4\chi_c(3-m)^{1/2}}{\sqrt{A_{TKE}}(1+m)}k^{(1+m)/2}\right] \quad (6.24)$$

(Poggi *et al.*, 2011). For the classical Kolmogorov inertial subrange (ISR) spectrum (Kolmogorov, 1941), given by $\phi_{TKE} = C_o\,(\varepsilon_{TKE})^{2/3}\,k^{-5/3}$, the scalar spectrum reduces to $\phi_{cc}(k) = (3C_o)^{-1/2}(\varepsilon_{TKE})^{1/3}\varepsilon_{cc}\left(k^{-5/3}\right)$ as $\chi_c \to 0$, in agreement with ISR theories for scalars. For the case of 2-D turbulence at scales experiencing a direct enstrophy cascade (or inverse energy cascade), $m \to 3$ and $\phi_{cc} \sim k^{-1}$, the outcome is consistent with the Batchelor spectrum for 2-D turbulence and passive scalars (Batchelor, 1959; Wells *et al.*, 2007). The spectral theory thus far assumes that the spectrum is dominated only by energy transfer and dissipation. In the case of canopy turbulence, ϕ_{TKE} may no longer be governed by clear scaling laws (as in the ISR) due to the work that the mean flow exercises against the foliage drag given as $W_p = \overline{u}^3/L_c$. The ability to infer $\tau(k)$ from $\phi_{TKE}(k)$ becomes difficult given that the canonical form of ϕ_{TKE} is not known *a priori*. In this case, phenomenological arguments and dimensional considerations would suggest that, at minimum, $\tau(k)$ must depend on W_p, the so-called enstrophy injection rate ($=\beta$) originating from the canopy elements, and wave number k. These dimensional considerations lead to $\tau(k) \sim \beta(C_d a_L \overline{u}^3)^{-1}k^{-2}$, which when inserted into the $\phi_{cc}(k)$ solution for an arbitrary $\tau(k)$, results in $\phi_{cc} \sim k^{-3}$ as $\chi_c \to 0$ (Poggi *et al.*, 2011). This k^{-3} scaling for canopies differs from the –3 power law first proposed for the inertial-diffusive range (Gibson, 1968) at very low Prandtl numbers ($=\nu/\chi_c$), where ν is the molecular viscosity.

To explore this canonical shape of the scalar spectrum when subjected to wake generation inside canopies, flume experiments were conducted in a recirculating constant head rectangular flume, 18 m long, 0.90 m wide, and 1 m deep (Poggi *et al.*, 2006, 2011). The water level was set to a steady and uniform value of 0.6 m. A canopy,

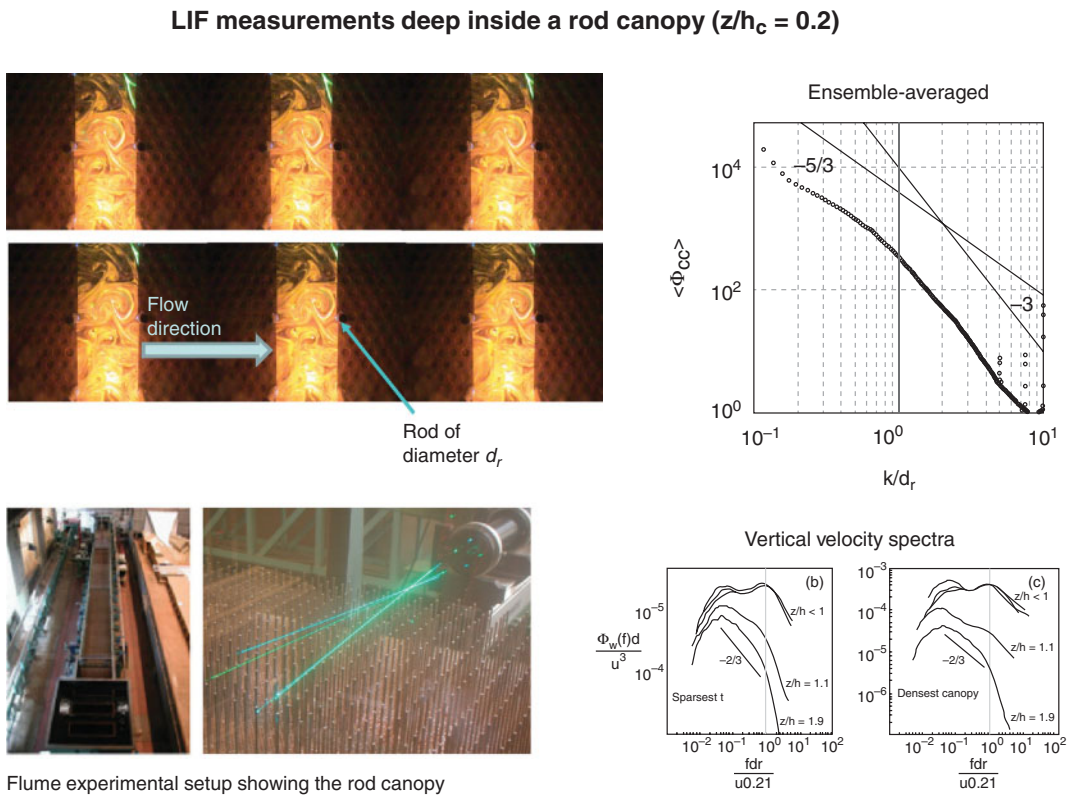

Figure 6.5 Top-left: Birds-eye view of LIF snap-shots illustrating the generation at the rod-scale (three rods in the vertical and two rods in the horizontal are visible per image) and advection of von Kármán streets deep inside the canopy ($z/h_c = 0.2$). Top-right: The ensemble-averaged ϕ_{cc} illustrating the scale at which the onset of a k^{-3} power-law occurs. Note that the k^{-3} scaling occurs at scales commensurate with or smaller than the rod diameter d_r. A near $k^{-5/3}$ is also evident for eddies larger than the rod diameter but smaller than the scale at which mechanical production is injected into the flow. Bottom: The flume and the rod-canopy system. The vertical velocity spectra (right) measured using laser-Doppler anemometry (also shown) across a wide range of canopy densities. Note that wake production and the short-circuiting of the Kolmogorov cascade occurs inside the canopy and across all heights and canopy densities.

composed of vertical cylinders that were 12 cm tall ($=h_c$) and 0.4 cm in diameter ($=d_r$) arrayed in a regular pattern at a density of 1072 rods m^{-2} was placed in a test section that was 9 m long and 0.9 m wide and was some 7 m downstream from the channel entrance (Poggi *et al.*, 2004). The canopy density was equivalent to a dense canopy having an element area index (frontal area per unit volume) of 4.27 m^2 m^{-2}. The measured C_d from these flume experiments were comparable to drag coefficients reported for dense forested ecosystems (Katul *et al.*, 2004). The local instantaneous dye concentration was measured using the laser-induced fluorescence (LIF) technique in a plane parallel to the channel bottom. The concentration measurements were conducted by injecting rhodamine 6G as a tracer, providing a horizontal light sheet between two lines of rods using a lens system, and recording a time sequence of images. Images were collected at $z/h_c = 0.2$ and recorded at 25 Hz using a colour CCD video camera at a spatial resolution of 0.00017 m (704 × 576 pixels). A sample sequence of an evolving Von Kármán street from this experiment is shown in Figure 6.5. Note that these vortices are able to traverse the rod spacing without much distortion from vertical turbulent fluctuations. The two-dimensional spectrum from each image was computed, normalized by the image variance, and the ensemble-average spectrum obtained over all the images was determined (see Figure 6.5). The $\phi_{cc} \sim k^{-5/3}$ for $k < d_r$ followed by an approximate $\phi_{cc} \sim k^{-3}$ scaling for $k > d_r$ agrees with the scaling analysis presented here given that enstrophy injection occurs at scales commensurate with d_r in these experiments. Hence, scalar dispersion at fine scales may share analogies with 2-D turbulence.

6.4.6 Scalar co-spectra

A simplified budget equation for the co-spectrum between the vertical velocity and scalars $\phi_{wc}(k)$ can be also analysed and is given by

$$\frac{\partial \phi_{wc}(k)}{\partial t} + (\nu + \chi_c) K^2 \phi_{wc}(k) = P(k) + T_{wc}(k) + \pi(k) \tag{6.25}$$

(Bos *et al.*, 2004), where $\int_0^\infty \phi_{wc}(k)dk = \overline{w'c'}$, $P(k) = (2/3)\Gamma_c \phi_{TKE}(k)$ is the production term due to a finite mean gradient (in the case of temperature, $\Gamma_c = \Gamma_T$), $T_{wc}(k)$ is the turbulent flux transport term across k, and $\pi(k)$ is the pressure-scalar covariance (a dissipation term) in the spectral domain. These terms mirror their counterparts in the scalar flux budget. As with the closure scheme earlier adopted for ϕ_{cc}, the most simplified representation for $\pi(k)$ is employed here for illustration, given by

$$\pi(k) = \frac{-A_\pi \phi_{wc}(k)}{\tau(k)} \tag{6.26}$$

(Bos *et al.*, 2004; Bos and Bertoglio, 2007) where A_π is a closure constant. Likewise, the transport term may be modelled, as with the case for the $\phi_{cc}(k)$ budget, via

$$T_{wc}(k) = -A_T \frac{\partial}{\partial k}\left(\frac{k\phi_{wc}(k)}{\tau(k)}\right). \tag{6.27}$$

Replacing these parameterizations in the co-spectral budget, ignoring the molecular diffusive and viscous terms, and defining a new variable given as $\Psi(k) = \phi_{wc}(k)/\tau(k)$, the co-spectral budget equation reduces to

$$\frac{\partial}{\partial k}(\Psi(k)) + \left(\frac{A_\pi}{A_T} + 1\right)\frac{1}{k}\Psi(k) = \frac{2}{3}\frac{\Gamma_c}{A_T}\frac{\phi_{TKE}(k)}{k}. \tag{6.28}$$

For a $\phi_{TKE} = A_{TKE}k^{-m}$, the above equation can be solved to yield

$$\Psi(k) = B_1 k^{-(1+A_\pi/A_T)} + \frac{2}{3}\frac{\Gamma_c}{A_T}\frac{1}{(1 + A_\pi/A_T - m)} \times A_{TKE}k^{-m} \tag{6.29}$$

where B_1 is an integration constant and $m < 1 + A_\pi/A_T$. If, as before, $\tau(k) = \left[(3-m)/(A_{TKE}k^{3-m})\right]^{1/2}$ (for $m < 3$), then

$$\phi_{wc}(k) = \sqrt{\frac{3-m}{A_{TKE}}}B_1 k^{-(5-m+2A_\pi/A_T)/2} + \frac{2}{3}\frac{\Gamma_c}{A_T}\frac{A_{TKE}^{1/2}\sqrt{3-m}}{(1 + A_\pi/A_T - m)}k^{-(m+3)/2}. \tag{6.30}$$

For a classical ISR, $A_{TKE} = C_o\varepsilon_{TKE}^{2/3}$, $m = 5/3$, $\tau(k) \sim k^{-2/3}$, and $\phi_{wc}(k) = \alpha_1 k^{-10/3-A_\pi/A_T} + \alpha_2 k^{-7/3}$ clearly dominated by the $k^{-7/3}$ term for large k. In fact, under these assumptions, this budget recovers the classical relation $\phi_{wc}(k) \sim \Gamma_c \varepsilon^{1/3} k^{-7/3}$. The above relation can also be expressed as

$$\phi_{wc}(k) \approx \left(\frac{2}{3}\frac{\Gamma_c}{A_T}\frac{1}{(1 + A_\pi/A_T - m)}\right)\phi_{TKE}(k)\tau(k) \tag{6.31}$$

and any power-law scaling in $\phi_{wc}(k)$ must be a superposition of a power-law scaling arising from the TKE spectrum and from the relaxation time scale (a measure of coherency in the flow). In the classical ISR, $\phi_{wc}(k) \sim k^{-5/3}k^{-2/3} \sim k^{-7/3}$ as discussed elsewhere (Lumley, 1967). It should be noted that very recent direct numerical simulations on passive scalars in a locally homogeneous and isotropic flow field did confirm the onset of a –7/3 scaling in the scalar-velocity co-spectrum (Gotoh and Watanabe, 2012) as well as a –5/3 scaling in the scalar spectrum.

Within the framework leading to equation (6.31) for the CSL, a number of distortions to the power-law exponents describing $\tau(k)$ and $\phi_{TKE}(k)$ arise. For example, $\tau(k)$ may be partially (or completely) decoupled from $\phi_{TKE}(k)$ so that $\tau(k) \neq (\int_0^k p^2\phi_{TKE}(p)dp)^{-1/2}$ as shown for the $\phi_{cc}(k)$ case when von Kármán streets dominate the flow (or even in an average sense as shown in Figure 6.2). Near $z/h_c = 1$, a number of studies have also shown nontrivial departures from $-5/3$ scaling for $\phi_{TKE}(k)$. These scaling arguments beg the provocative question as to what extent the canopy distortions of the classical ISR, especially above the canopy, perturb the $-7/3$ scalar-velocity co-spectral exponents. To address this issue, it is instructive to recast Equation (6.31) with the following scaling arguments: if $\phi_{TKE}(k) \sim k^{-m}$ and $\tau(k) \sim k^{-n}$, then $\phi_{wc}(k) \sim k^{-\omega}$ with $\omega = m + n$. Next, the degree of departure from the $-7/3$ scaling are decomposed into departures in the TKE scaling from $m = 5/3$ and departures in the relaxation time scale from $n = 2/3$. This argument assumes *a priori* that $\tau(k)$ is decoupled from $\phi_{TKE}(k)$ as indirectly supported in Figure 6.2 and the $\phi_{cc}(k)$ analysis. Recall that when $\tau(k)$ is entirely coupled to $\phi_{TKE}(k)$, then $\omega = -(m/2 + 3/2)$. Despite their immediate connections to the coherency in the flow, the $\tau(k)$ spectra are rarely measured or reported in the atmosphere. However, velocity spectra and scalar-velocity co-spectra are routinely measured. By regressing measured ω upon measured m and analysing the regression statistics of the equation $\omega = a_w m + b_w$ and exploring whether $a_w = 0.5$ or $a_w = 1.0$, and $b_w = 2/3$

or 3/2, the degree of coupling between $\phi_{TKE}(k)$ and $\tau(k)$ can be quantified within the CSL. Such analysis was carried out for velocity and multiple scalar concentration turbulence measurements (temperature, water vapour, and CO_2) collected above three tall forested ecosystems, where the measurement height (z_m) is situated within the CSL ($1 < z_m/h_c < 2$). Atmospheric stability conditions were classified as neutral to weakly unstable when $-0.5 < \zeta_{st} \leq 0$ and neutral to weakly stable when $0 \leq \zeta_{st} < 0.5$, where $\zeta_{st} = (z_m - d)/L_{mo}$, d is the zero-plane displacement (=0.67 h_c), and L_{mo} is the Obukhov length. Details about the sites, data sets, and their processing for the Loblolly pine forest ($h_c = 19$ m, LAI = 5.5, $z_m = 20.2$ m), the oak-hickory hardwood forest ($h_c = 25$ m, LAI = 6, $z_m = 40$ m), and the alpine hardwood canopy ($h_c = 28$ m, LAI = 9, $z_m = 33$ m), are discussed elsewhere (Cava and Katul, 2009; Cava *et al.*, 2012). Figure 6.6 shows the ensemble-averaged measured velocity and scalar spectra and vertical velocity-scalar co-spectra above these three canopies and for all three scalars.

The expected ISR scaling laws are also shown in Figure 6.6. It is clear that the scalar co-spectra do not decay as fast as –7/3 within the ISR (roughly, the region delineated by frequencies where the vertical velocity follows an approximate –5/3 scaling) despite the fact that the velocity component co-spectrum decays at –7/3 with increasing frequency. To what extent the departures from –7/3 in the scalar co-spectra can be explained by the departure from -5/3 in the vertical velocity spectra is explored in Figure 6.7. It is clear from the analysis in Figure 6.7 that, to a first order, the departures in the scalar co-spectrum exponent can be partly (though not completely) explained by the departure in the vertical velocity spectrum. Moreover, the data here are suggestive that the slope and intercept of the relation $\omega = a_w m + b_w$ are closer to $a_w = 1.0$ and $b_w = 2/3$ than $a_w = 0.5$ and $b_w = 3/2$. Hence, it appears that $\tau(k) \sim k^{-2/3}$ despite departures from $m = 5/3$ in the velocity. This necessarily implies that the spectrum of the dissipation rate must also be adjusting beyond its inertial value in the CSL, which was already anticipated from the

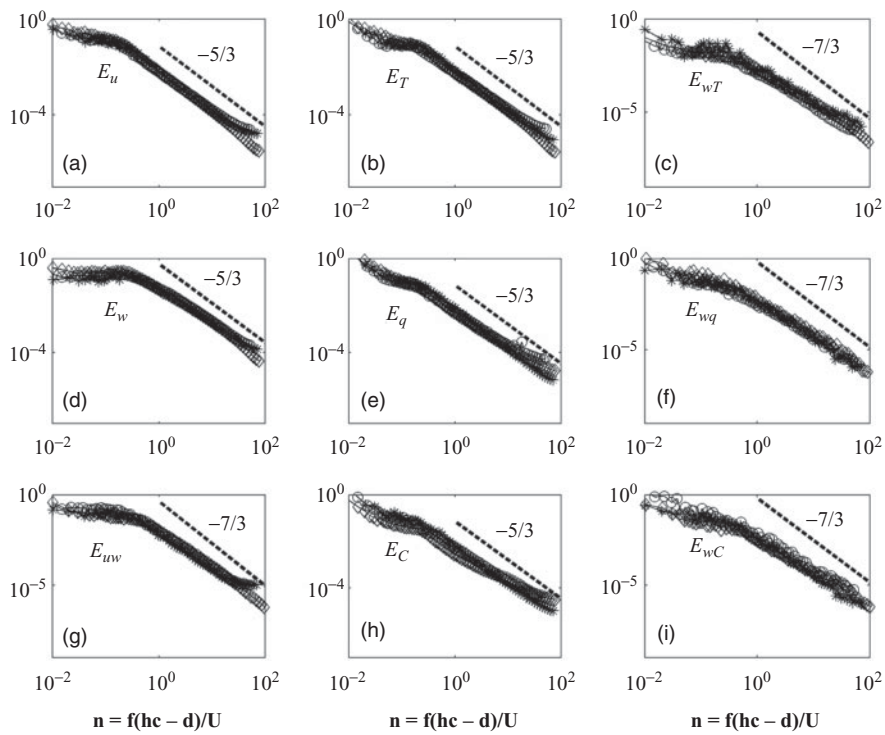

Figure 6.6 Ensemble-averaged normalized spectra and co-spectra of the velocity and scalars (T for temperature, q for water vapour, and C for CO_2) measured *above* an alpine hardwood forest in Lavarone, Italy (diamonds), oak-hickory forest in North Carolina, United States (circles), and a Pine forest in North Carolina, United States (stars) as a function of the dimensionless frequency n, where h_c is the canopy height, d is the zero-plane displacement, and U is the mean velocity. Dashed lines represent the power laws predicted from Kolmogorov's theory in the inertial subrange for the velocity spectrum (–5/3) and velocity-scalar co-spectrum (–7/3).

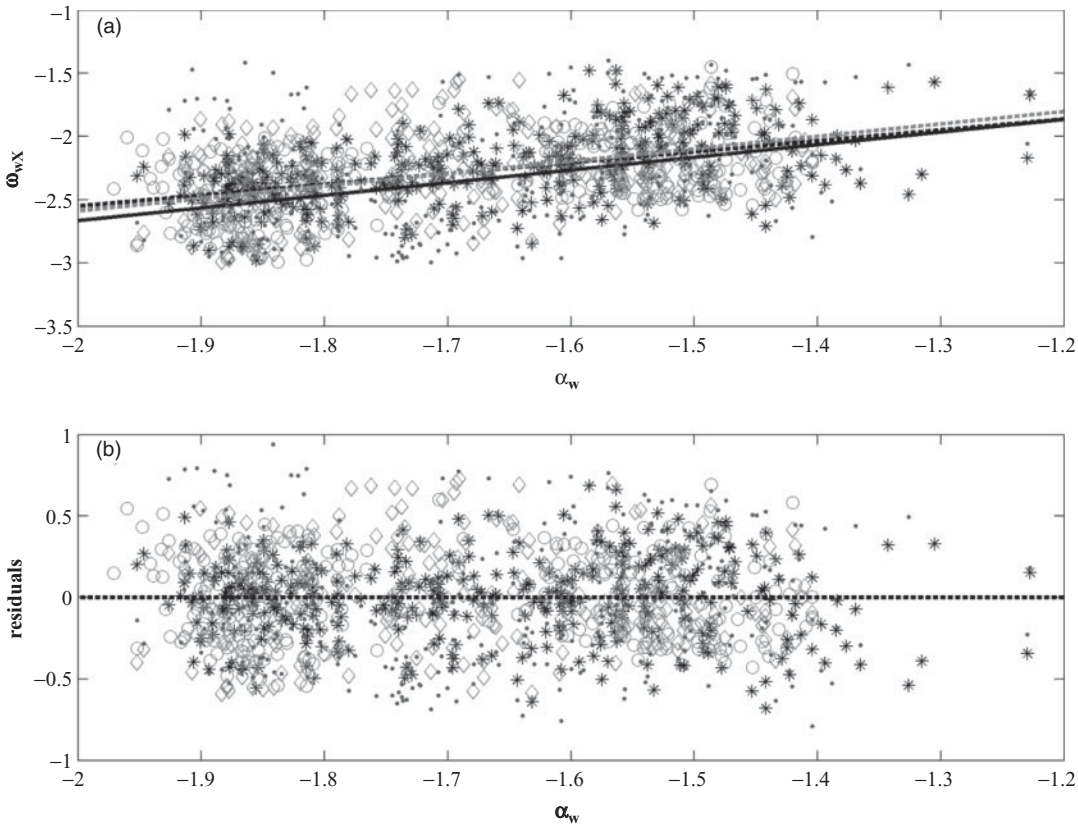

Figure 6.7 (a) Scatter plot of spectral exponent of vertical velocity components (α) against cospectral exponents (ω) of uw (points), wT (stars), wq (grey diamonds) and wC (grey circles). Continuous black line refers to the proposed linear relation between spectral exponents ($\omega = \alpha$–2/3); black dotted line refers to linear fit relative only to uw cospectra ($\omega = 0.98\alpha$-0.62; R = 0.38); grey dotted line refers to the linear fit relative to all scalar data sets (wT, wq, wC cospectral exponents against w spectral exponent) ($\omega = 0.86\alpha$–0.83; R = 0.45). (b) Residuals relative to the computed linear fits shown in Figure 6.7a.

flume experiments in Figure 2 (i.e. $\partial\tau/\partial z \neq k_v/u_*$ or even constant for that matter in the CSL).

Thus far, the work presented here has dealt with scalar spectra and velocity-scalar co-spectra at $kh_c \gg 1$. Next, the structure of scalar turbulence for eddies commensurate with h_c and possible effects on scalar spectra at scales $kh_c >> 1$ are briefly considered.

6.4.7 Scalar fluxes, fine-scale turbulence and ramp patterns

Numerous studies have reported that scalar concentration time series measured above vegetated and nonvegetated surfaces exhibit a repeating ramp (or inverse ramp) pattern characterized by a gradual rise (or decrease) followed by a relatively sharp drop (or rise). These ramp-like features are generally absent in the concomitant $u'(t)$ series, suggesting that they are properties of coherent scalar turbulence at large scales. These structures have been observed in nonthermally stratified boundary layer flows over smooth walls and rough walls (Warhaft, 2000), and in canopy large eddy simulation runs (Fitzmaurice *et al.*, 2004). For CSL flows, ramp patterns have also been reported within and above canopies (Bergstrom and Hogstrom, 1989; Shaw *et al.*, 1989; Paw U *et al.*, 1992; Cava *et al.*, 2004; Thomas and Foken, 2007; Zhang *et al.*, 2011), indicating eddy coherence at scales commensurate with h_c. Moreover, ramp (or inverse ramp) patterns have been noted at all atmospheric stability regimes and for multiple scalars (Shaw *et al.*, 1989; Collineau and Brunet, 1993; Brunet and Irvine, 2000; Cava *et al.*, 2004), including mildly stable stratified atmospheric conditions. In fact, depending on whether the canopy is a source or a sink of a scalar entity, ramps or inverse ramps exist as shown in Figure 6.8. For the nocturnal temperature trace

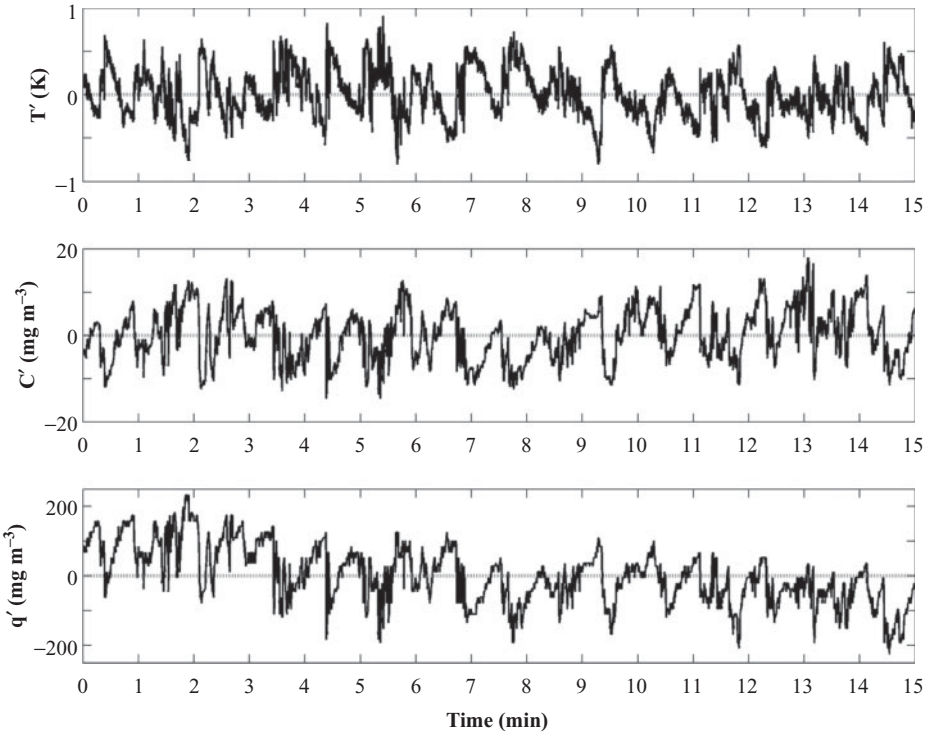

Figure 6.8 Time series of air temperature, CO_2 and water vapour concentration fluctuation measured above a Loblolly pine forest during mildly stable conditions at night. Note the inverse ramp patterns when $\overline{w'T'} < 0$ and the regular ramp patterns when $\overline{w'q'}$ or $\overline{w'C'} > 0$ (nocturnal ecosystem respiration and evaporation).

in Figure 6.8, the canopy is a sink of heat and inverse ramps prevail in the temperature time series. For these same nocturnal conditions, the canopy is a source of CO_2 due to the fact that respiration dominates the flux in the absence of any leaf photosynthesis (as expected when the incident photosynthetically active radiation is small). Moreover, the canopy is generally a small source of water vapour at night, as evidenced by a large number of studies (Novick *et al.*, 2009). For the latter two scalars, Figure 6.8 shows that regular ramps, identical to those reported in heated laboratory boundary layers, emerge (Warhaft, 2000).

Scalar ramps have also been shown to contribute significantly to the turbulent flux (Shaw *et al.* 1989; Paw U *et al.*, 1992, 1995; Katul *et al.*, 1996; Spano *et al.*, 1997, 2000; Castellvi *et al.*, 2002, 2006). However, a clear phenomenological theory that predicts their onset has been lacking.

As early as 1935, Higbie proposed a surface renewal theory to investigate interfacial heat transfer between a liquid and a gas (Higbie, 1935); this approach is now gaining some popularity in micrometeorology and surface hydrology (Paw U *et al.*, 1995; Katul *et al.*, 1996; Spano *et al.*, 1997; Spano *et al.*, 2000; Castellvi *et al.*, 2006). Higbie visualized heat transport as occurring by the arrival of fresh transporting fluid elements originating from the bulk fluid above a heated surface, followed by an unsteady diffusion transport during surface contact (or residence time) between these fluid elements and the surface, and finally the eventual replacement of the stale element by a fresh fluid from aloft. Figure 6.9 shows schematically the Higbie surface renewal framework extended to a canopy for CO_2, leading to a 'ramp-like' motion (Paw U *et al.*, 1995). The size of these ramps above the canopy varies with thermal stratification, with a minimum size at or near neutral condition and increases as the stability regimes shifts to either unstable or stable conditions (Lu and Fitzjarrald, 1994; Barthlott *et al.*, 2007; Zhang *et al.*, 2011).

The implications of such a ramp-like pattern on the fine scale structure of scalars within the ISR and on scalar flux models conclude this review. With regards to the ISR, it was noted by Warhaft that 'while the ramp-cliff structures

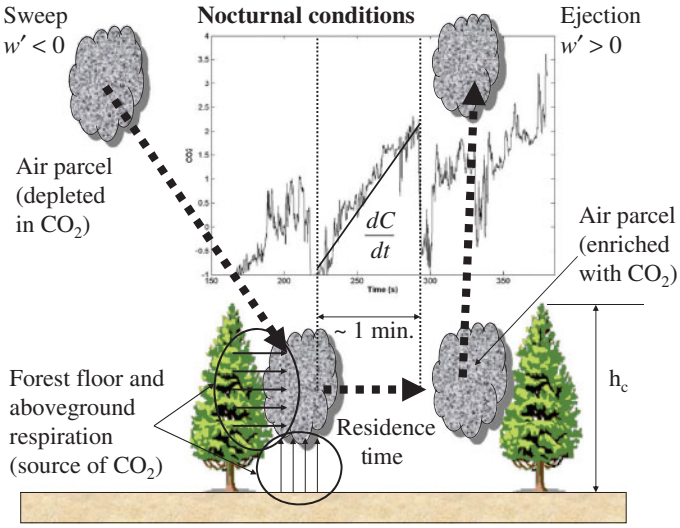

Figure 6.9 Illustration of the connection between the ramp-like patterns in the turbulent scalar concentration time series, the ejection-sweep cycle, and the renewal process using nocturnal CO_2 concentration measurements collected just above a pine forest ($z/h_c = 1.12$). Parcels of air, comparable to the canopy height, with ambient CO_2 concentration sweep into the canopy ($w' < 0$), reside within the canopy volume for about 1 minute, and eject out ($w' > 0$), imprinting a 'ramp-like' structure in the scalar concentration time series shown. During nocturnal conditions, above ground biomass (including foliage and woody components) and forest floor are both respiring (i.e. sources of CO_2).

are large-scale features, on the order of an integral scale, the front itself is sharp, and thus is manifested at the small scales' (Warhaft, 2000). Subsequent experiments suggest that this sharp front becomes even sharper at higher Taylor microscale Reynolds numbers, thereby compounding its effects on the ISR (especially in the atmosphere). The presence of ramps was also used to explain why intermittency correction parameters to Kolmogorov's 1941 theories for the ISR appear larger for scalars when compared to velocity (Mahrt and Gibson, 1992; Mahrt and Howell, 1994; Warhaft, 2000; Katul *et al.*, 2006b). One such analysis made use of Tsallis's nonextensive thermostatistics (Tsallis, 1988; Bolzan *et al.*, 2002; Ramos *et al.*, 2004), which provided a unifying framework to investigate two inter-connected problems: similarity between scalars and velocity statistics within the inertial subrange and 'contamination' of internal intermittency by 'external' factors. It was shown that conventional 'internal' intermittency models, including the She–Leveque, Lognormal, and Log-stable, reproduce well the observed Tsallis parameters for velocity statistics within the inertial subrange, but fail to describe the fluctuations for the scalars (Katul *et al.*, 2006b). Scalars also appear more intermittent than velocity when the underlying surface is a large source or sink, thereby confirming an 'external' intermittency contribution. In fact, numerical experiments in which a synthetic time series was composed of a linear superposition of a mono-fractal process (such as fractional Brownian motion) and a periodic ramp-like trace exhibited large intermittency corrections resembling those of scalars (Katul *et al.*, 2006b). These findings agree with recent Large Eddy Simulation studies applied to the atmospheric boundary layer (Mazzitelli and Lanotte, 2012).

Another line of research uses the presence of ramps as a practical method to infer sensible heat flux from temperature traces, as first proposed by Paw U and coworkers (Paw U *et al.*, 1995). Because temperature traces are more convenient to acquire than simultaneous air temperature and velocity series, the method does offer practical advantages over eddy-covariance approaches. The basic premise is that, in a Lagrangian frame of reference, a parcel of air will change its air temperature due to molecular diffusion of heat into or out of the parcel volume or collisions with a heat source resulting in

$$\frac{dT}{dt} = \chi_T \frac{\partial^2 T}{\partial x_j \partial x_j} + S_T \tag{6.32}$$

where repeated indices imply summation, as common in index notation. If the Peclet number is sufficiently large, then the heat loss or gain by molecular diffusion can be ignored and the air parcel will experience a change in temperature only when it exchanges heat with a source S_T. To transpose this Lagrangian view to a Eulerian frame of reference

$$\frac{dT}{dt} = \frac{\partial T}{\partial t} + u_j \frac{\partial T}{\partial x_j} \approx S_T \tag{6.33}$$

where T and u_j are the instantaneous temperature and velocity. High-frequency Eulerian measurements of air temperature provide estimates only of $\partial T/\partial t$. However, as argued elsewhere (Paw U *et al.*, 1995; Katul *et al.*, 1996), because $u_j \partial T/\partial x_j$ is a product, its significance must be

at frequencies higher than those governing T. For example, if $u \sim e^{i\theta_1}$ and $T \sim e^{i\theta_2}$, then $uT \sim e^{i(\theta_1+\theta_2)}$, which is at a higher frequency than T. With the assumptions that the ramp time scale is sufficiently long (e.g. 1 minute in Figure 6.9), contributions to $u_j \partial T/\partial x_j$ can be ignored at those timescales. Furthermore, assuming that the volume of the air parcel is coherent, commensurate with the canopy volume, and the temperature in the ramp is well mixed,

$$\frac{V_a}{A_g}\frac{\partial T}{\partial t} \approx \int_0^{h_c} S_T(z)dz \tag{6.34}$$

where V_a is the air volume associated with the ramp and A_g is the ground area. Here, the ground is treated as a source (instead of a flux), and eddies producing the ramp pattern fully penetrate the canopy and touch the ground. If $V_a/A_g \approx h_c$, and upon conditionally sampling the series to infer $\partial T/\partial t$ only during its residence time in the canopy (Figure 6.9), then the method can yield estimates of scalar fluxes from the mean rise or mean drop of the ramp structure. A number of studies reported some success in using this approach to infer sensible heat provided some calibration is carried out (Spano *et al.*, 1997; Spano *et al.*, 2000; Castellvi *et al.*, 2002, 2006; Castellvi, 2004). While the practicalities and calibration parameters of this method, now known as surface renewal analysis, are still being worked-out, the theoretical appeal that coherent motions in the scalar field explain much of the scalar fluxes is quite seductive.

6.5 Summary and conclusions

The bulk and spectral properties of scalar turbulence within the canopy sublayer (CSL) have been presented. A unifying Eulerian framework that bridges between a number of arguments generally invoked to explain the failure of gradient diffusion theory ($\overline{w'T'} \sim \partial\overline{T}/\partial z$) in the scalar field was proposed for the CSL. It was shown that 'closing' the flux-transport term via the most primitive local gradient-diffusion scheme (i.e. $\overline{w'w'T'} \sim \partial\overline{w'T'}/\partial z$) explicitly reveals why the near-field effects in the scalar source impact gradient-diffusion theory. Upon linking the (same) flux-transport term to the ejection-sweep cycle via a cumulant expansion method, the explicit causal link between coherent structures and the failure of gradient diffusion can be unlocked. Another benefit to the proposed framework is the role of the scalar variance (connected to the buoyancy term) in the failure of gradient diffusion theory, which cannot be readily predicted by Lagrangian methods.

A defining syndrome of canopy turbulence, especially deep inside the canopy, is the significant role of wake generation. The effects of these wakes on the mean and turbulent kinetic energies as well as the spectral short-circuiting have been studied. However, a theory that attempts to predict the shape of the scalar spectrum following the injection of wake energy remains lacking. A novel theoretical argument complemented by results from flume experiments presented here showed that, at scales larger than the wake energy injection scale, the scalar spectrum scales as k^{-3}. These predictions agree with flume experiments when the canopy is composed of densely arrayed steel rods with uniform diameters. The co-spectral properties between scalar fluctuations and the vertical velocity at scales larger than the shear injection scale ($\sim h_c$) were also explored. It was shown that the co-spectral departures from the classical $-7/3$ scaling law can be partly explained by departures in the spectrum of the vertical velocity from $-5/3$, provided the relaxation time scale spectrum does not appreciably diverge from its $k^{-2/3}$ value.

Finally, the presence of ramp-like signatures at scales commensurate with h_c was briefly reviewed. It was shown that a renewal process can phenomenologically explain the shape of ramps. This same phenomenological theory can be used to predict scalar fluxes from high-frequency scalar concentration time series, provided proper calibration and ramp identification schemes in the time series (especially during the sweeping and residence phases) are employed. The presence of ramps on the enhancement of fine-scale intermittency due to external factors was also briefly covered.

6.6 Acknowledgements

The authors thank Mike Church and the anonymous referee for all the helpful comments and suggestions. Katul acknowledges the support from the National Science Foundation (through EAR–1013339, AGS-110227, CBET-103347), the US Department of Energy through the Office of Biological and Environmental Research (BER) Terrestrial Ecosystem Science (TES) program (DE-SC0006967), the US Department of Agriculture (2011-67003-30222), and the Binational Agricultural Research and Development (BARD) Fund (IS-4374-11C). Cava acknowledges the support from Cooperazione Italia-USA su Scienza e Tecnologia

dei Cambiamenti Climatici, Anno 2006–2008. Poggi acknowledges the support from the Commission of the European Communities's WARECALC program (PIRSES-GA-2008-230845). Siqueira acknowledges the support from Conselho Nacional de Desenvolvimento Científico e Tecnologico (CNPq) of Brazil, process number 306525/2010-0.

References

Antonia, R.A. (1981) Conditional sampling in turbulence measurements. *Annual Review of Fluid Mechanics* **13**, 131–156.

Baldocchi, D., Falge, E., Gu, L.H. *et al.* (2001) FLUXNET: A new tool to study the temporal and spatial variability of ecosystem-scale carbon dioxide, water vapor, and energy flux densities. *Bulletin of the American Meteorological Society* **82**, 2415–2434.

Barthlott, C., Drobinski, P., Fesquet, C. *et al.* (2007) Longterm study of coherent structures in the atmospheric surface layer. *Boundary Layer Meteorology* **125**, 1–24.

Bash, J.O., Walker, J.T., Katul, G.G. *et al.* (2010) Estimation of in-canopy ammonia sources and sinks in a fertilized zea mays field. *Environmental Science and Technology* **44**, 1683–1689.

Batchelor, G. (1959) Small-scale variation of convected quantities like temperature in turbulent fluid. Part 1. General discussion and the case of small conductivity. *Journal of Fluid Mechanics* **5**, 113–133.

Belcher, S.E., Harman, I.N. and Finnigan, J.J. (2012) The wind in the willows: flows in forest canopies in complex terrain. *Annual Review of Fluid Mechanics* **44**, 479–504.

Belcher, S.E. and Hunt, J.C.R. (1998) Turbulent flow over hills and waves. *Annual Review of Fluid Mechanics* **30**, 507–538.

Belcher, S.E., Jerram, N. and Hunt, J.C.R. (2003) Adjustment of a turbulent boundary layer to a canopy of roughness elements. *Journal of Fluid Mechanics* **488**, 369–398.

Bergstrom, H. and Hogstrom, U. (1989) Turbulent exchange above a pine forest: 2. Organized structures. *Boundary-Layer Meteorology* **49**, 231–263.

Bolzan, M.J.A., Ramos, F.M., Sa, L.D.A. *et al.* (2002) Analysis of fine-scale canopy turbulence within and above an Amazon forest using Tsallis' generalized thermostatistics. *Journal of Geophysical Research-Atmospheres* **107**, 8063. DOI: 10.1029/2001JD000378.

Bos, W.J.T. and Bertoglio, J.P. (2007) Inertial range scaling of scalar flux spectra in uniformly sheared turbulence. *Physics of Fluids* **19**, 025104.

Bos, W.J.T., Touil, H., Shao, L. and Bertoglio, J.P. (2004) On the behavior of the velocity-scalar cross correlation spectrum in the inertial range. *Physics of Fluids* **16**, 3818–3823.

Brunet, Y. and Irvine, M.R. (2000) The control of coherent eddies in vegetation canopies: streamwise structure spacing, canopy shear scale and atmospheric stability. *Boundary Layer Meteorology* **94**, 139–163.

Castellvi, F. (2004) Combining surface renewal analysis and similarity theory: a new approach for estimating sensible heat flux. *Water Resources Research* **40**, W05201. DOI: 10.1029/2003WR002677.

Castellvi, F., Perez, P.J. and Ibanez, M. (2002) A method based on high-frequency temperature measurements to estimate the sensible heat flux avoiding the height dependence. *Water Resources Research* **38**, 6. DOI: 10.1029/2001WR000486.

Castellvi, F., Snyder, R.L., Baldocchi, D.D. and Martinez-Cob, A. (2006) A comparison of new and existing equations for estimating sensible heat flux using surface renewal and similarity concepts. *Water Resources Research* **42**, W08406. DOI: 10.1029/2005WR004642.

Cava, D., Giostra, U., Siqueira, M. and Katul, G. (2004) Organised motion and radiative perturbations in the nocturnal canopy sublayer above an even-aged pine forest. *Boundary-Layer Meteorology* **112**, 129–157.

Cava, D. and Katul, G.G. (2009) The effects of thermal stratification on clustering properties of canopy turbulence. *Boundary-Layer Meteorology* **130**, 307–325.

Cava, D., Katul, G., Molini, A. and Elefant, C. (2012) The role of surface characteristics on intermittency and zero-crossing properties of atmospheric turbulence. *Journal of Geophysical Research* **117**, D01104. DOI: 10.1029/2011JD016167.

Cava, D., Katul, G.G., Scrimieri, A. *et al.* (2006) Buoyancy and the sensible heat flux budget within dense canopies. *Boundary-Layer Meteorology* **118**, 217–240.

Chameides, W., Kasibhatla, P., Yienger, J. and Levy, H. (1994) Growth of continental-scale metro-agro-plexes, regional ozone pollution, and world food-production. *Science* **264**, 74–77.

Collineau, S. and Brunet, Y. (1993) Detection of turbulent coherent motions in a forest canopy: 1. Wavelet analysis. *Boundary-Layer Meteorology* **65**, 357–379.

Corssin, S. (1964) Further generalization of Onsager's cascade model for turbulent spectra. *Physics of Fluids* **7**, 1156.

Corrsin, S. (1974) Limitations of gradient transport models in random walks and in turbulence. *Advances in Geophysics* **18A**, 25–60.

Danaila, L. and Antonia, R.A. (2009) Spectrum of a passive scalar in moderate Reynolds number for homogeneous isotropic turbulence. *Physics of Fluids* **21**, 111702.

de Langre, E. (2008) Effects of wind on plants. *Annual Review of Fluid Mechanics* **40**, 141–168.

Finnigan, J. (2000) Turbulence in plant canopies. *Annual Reviews of Fluid Mechanics* **32**, 519–571.

Finnigan, J.J., Shaw, R.H. and Patton, E.G. (2009) Turbulence structure above a vegetation canopy. *Journal of Fluid Mechanics* **637**, 387–424.

Fitzmaurice, L., Shaw, R.H., Paw U, K.T. and Patton, E.G. (2004) Three-dimensional scalar microfront systems in a

large-eddy simulation of vegetation canopy flow. *Boundary-Layer Meteorology* **112**, 107–127.

Frenkiel, F. and Klebanoff, P. (1967) Higher order correlations in a turbulent field. *Physics of Fluids* **10**, 507–522.

Gao, W. and Wesely, M.L. (1993) Numerical modeling of the turbulent fluxes of chemically reactive trace gases in the atmospheric boundary layer. *Journal of Applied Meteorology* **33**, 835–847.

Gao, W., Wesely, M.L. and Doskey, P.V. (1993) Numerical modeling of the turbulent diffusion and chemistry of NOx, O3, isoprene, and other reactive trace gases in and above a forest canopy. *Journal of Geophysical Research* **98**, 339–353.

Garratt, J.R. (1992) *The Atmospheric Boundary Layer*, Cambridge University Press, Cambridge.

Gibson, C. (1968) Fine structure of scalar fields mixed by turbulence. II. Spectral theory. *Physics of Fluids* **11**, 2316.

Gotoh, T. and Watanabe, T. (2012) Scalar flux in a uniform mean scalar gradient in homogeneous isotropic steady turbulence. *Physica D – Nonlinear Phenomena* **241**, 141–148.

Harman, I.N. and Finnigan, J.J. (2007) A simple unified theory for flow in the canopy and roughness sublayer. *Boundary-Layer Meteorology* **123**, 339–363.

Harman, I.N. and Finnigan, J.J. (2008) Scalar concentration profiles in the canopy and roughness sublayer. *Boundary-Layer Meteorology* **129**, 323–351.

Higbie, R. (1935) The rate of absorption of a pure gas into a still liquid during short periods of exposure. *Transactions of the American Institute of Chemical Engineers* **31**, 365–389.

Katul, G.G. and Albertson, J.D. (1999) Modeling CO_2 sources, sinks, and fluxes within a forest canopy. *Journal of Geophysical Research – Atmospheres* **104**, 6081–6091.

Katul, G.G. and Poggi, D. (2011) A note on aerosol sized particle deposition onto dense and tall canopies situated on gentle cosine hills. *Tellus Series B – Chemical and Physical Meteorology* **63**, 395–400.

Katul, G.G., Poggi, D. and Ridolfi, L. (2011) A flow resistance model for assessing the impact of vegetation on flood routing mechanics. *Water Resources Research* **47**, W08533. DOI: 10.1029/2010WR010278.

Katul, G.G., Konings, A.G. and Porporato, A. (2011) Mean velocity profile in a sheared and thermally stratified atmospheric boundary layer. *Physical Review Letters* **107**, 268502.

Katul, G.G., Mahrt, L., Poggi, D. and Sanz, C. (2004) One- and two-equation models for canopy turbulence. *Boundary-Layer Meteorology* **113**, 81–109.

Katul, G., Poggi, D., Cava, D. and Finnigan, J. (2006a) The relative importance of ejections and sweeps to momentum transfer in the atmospheric boundary layer. *Boundary-Layer Meteorology* **120**, 367–375.

Katul, G., Porporato, A., Cava, D. and Siqueira, M. (2006b) An analysis of intermittency, scaling, and surface renewal in atmospheric surface layer turbulence. *Physica D – Nonlinear Phenomena* **215**, 117–126.

Katul, G., Hsieh, C.I., Oren, R. *et al.* (1996) Latent and sensible heat flux predictions from a uniform pine forest using surface renewal and flux variance methods. *Boundary-Layer Meteorology* **80**, 249–282.

Katul, G.G., Finnigan, J.J., Poggi, D. *et al.* (2006c) The influence of hilly terrain on canopy-atmosphere carbon dioxide exchange. *Boundary-Layer Meteorology* **118**, 189–216.

Katul, G., Oren, R., Ellsworth, D. *et al.* (1997) A Lagrangian dispersion model for predicting CO2 sources, sinks, and fluxes in a uniform loblolly pine (Pinus taeda L) stand. *Journal of Geophysical Research – Atmospheres* **102**, 9309–9321.

Katul, G., Lai, C.T., Schafer, K. *et al.* (2001) Multiscale analysis of vegetation surface fluxes: from seconds to years. *Advances in Water Resources* **24**, 1119–1132.

Kolmogorov, A.N. (1941) The local structure of turbulence in incompressible viscous fluid for very large Reynolds number. *Doklady Akademiia Nauk SSSR* **30**, 9–13.

Lin, M., Katul, G. and Khlystov, A. (2012) A branch scale analytical model for predicting the vegetation collection efficiency of ultrafine particles. *Atmospheric Environment* **51**, 293–302. DOI: 10.1016/j.atmosenv.2012.1001.1004.

Lu, C.H. and Fitzjarrald, D.R. (1994) Seasonal and diurnal variations of coherent structures over a deciduous forest. *Boundary Layer Meteorology* **69**, 43–69.

Lu, S.S. and Willmarth, W.W. (1973) Measurements of the structure of Reynolds stress in a turbulent boundary layer. *Journal of Fluid Mechanics* **60**, 481–571.

Lumley, J.L. (1967) Similarity and the turbulent energy spectrum. *Physics of Fluids* **10**, 855–858. DOI: org/10.1063/1.1762201.

Mahrt, L. and Gibson, W. (1992) Flux decomposition into coherent structures. *Boundary-Layer Meteorology* **60**, 143–168.

Mahrt, L. and Howell, J.F. (1994) The influence of coherent structures and microfronts on scaling laws using global and local transforms. *Journal of Fluid Mechanics* **260**, 247–270.

Malhi, Y. (2002) Carbon in the atmosphere and terrestrial biosphere in the 21st century. *Philosophical Transaction of the Royal Society* **A360**, 2925–2945.

Manzoni, S., Katul, G., Fay, P.A. *et al.* (2011) Modeling the vegetation-atmosphere carbon dioxide and water vapor interactions along a controlled CO(2) gradient. *Ecological Modelling* **222**, 653–665.

Mazzitelli, I. and Lanotte, A.S. (2012) Active and passive scalar intermittent statistics in turbulent atmospheric convection. *Physica D – Nonlinear Phenomena* **241**, 251–259.

Meyers, T. and Paw U, K.T. (1986) Testing of a higher-order closure model for modeling air flow within and above plant canopies. *Boundary Layer Meteorology* **37**, 297–311.

Meyers, T. and Paw U, K.T. (1987) Modelling the plant canopy micrometeorology with higher-order closure principles. *Agricultural and Forest Meteorology* **41**, 143–163.

Monin, A.S. and Obukhov, A.M. (1954) Basic laws of turbulent mixing in the surface layer of the atmosphere. Akademiia Nauk SSSR, *Trudy Geophiz. Inst.* **24**, 163–187.

Nakagawa, H. and Nezu, I. (1977) Prediction of the contributions to the Reynolds stress from bursting events in open channel flows. *Journal of Fluid Mechanics* **80**, 99–128.

Nathan, R., Katul, G.G., Bohrer, G. *et al.* (2011) Mechanistic models of seed dispersal by wind. *Theoretical Ecology* **4**, 113–132.

Nathan, R., Katul, G., Horn, H. *et al.* (2002) Mechanisms of long-distance dispersal of seeds by wind. *Nature* **418**, 409– 413.

Nepf, H. (2012) Flow and transport in regions with aquatic vegetation. *Annual Review of Fluid Mechanics* **44**, 123–142. DOI: 10.1146/annurev-fluid-120710-101048.

Novick, K., Oren, R., Stoy, P. *et al.* (2009) Nocturnal evapotranspiration in eddy-covariance records from three co-located ecosystems in the Southeastern US: Implications for annual fluxes. *Agricultural and Forest Meteorology* **149**, 1491–1504.

Paw U, K.T., Brunet, Y., Collineau, S. *et al.* (1992) On coherent structures in turbulence above and within agricultural plant canopies. *Agricultural and Forest Meteorology* **61**, 55–68.

Paw U, K.T., Qiu, J., Su, H.B. *et al.* (1995) Surface reneal analysis: a new method to obtain scalar fluxes. *Agricultural and Forest Meteorology* **74**, 119–137.

Petroff, A., Mailliat, A., Amielh, M. and Anselmet, F. (2008) Aerosol dry deposition on vegetative canopies. Part I: Review of present knowledge. *Atmospheric Environment* **42**, 3625–3653.

Pierce, J.R. and Adams, P.J. (2007) Efficiency of cloud condensation nuclei formation from ultrafine particles. *Atmospheric Chemistry and Physics* **7**, 1367–1379.

Poggi, D. and Katul, G. (2009) Flume experiments on intermittency and zero-crossing properties of canopy turbulence. *Physics of Fluids* **21**, 065103.

Poggi, D., Katul, G. and Albertson, J. (2006) Scalar dispersion within a model canopy: Measurements and three-dimensional Lagrangian models. *Advances in Water Resources* **29**, 326–335.

Poggi, D., Katul, G.G. and Cassiani, M. (2008) On the anomalous behavior of the Lagrangian structure function similarity constant inside dense canopies. *Atmospheric Environment* **42**, 4212–4231.

Poggi, D., Katul, G.G. and Vidakovic, B. (2011) The role of wake production on the scaling laws of scalar concentration fluctuation spectra inside dense canopies. *Boundary-Layer Meteorology* **139**, 83–95.

Poggi, D., Porporato, A., Ridolfi, L. *et al.* (2004) The effect of vegetation density on canopy sub-layer turbulence. *Boundary-Layer Meteorology* **111**, 565–587.

Ramos, F.M., Bolzan, M.J.A., Sa, L.D.A. and Rosa, R.R. (2004) Atmospheric turbulence within and above an Amazon forest. *Physica D – Nonlinear Phenomena*, **193**, 278–291.

Raupach, M. (1981) Conditional statistics of Reynolds stress in rough-wall and smooth-wall turbulent boundary layers. *Journal of Fluid Mechanics* **108**, 363–382.

Raupach, M. (1989) Applying Lagrangian fluid-mechanics to infer scalar source distributions from concentration profiles in plant canopies. *Agriculture and Forest Meteorology* **47**, 85–108.

Raupach, M., Finnigan, J.J. and Brunet, Y. (1996) Coherent eddies and turbulence in vegetation canopies: The mixing-layer analogy. *Boundary-Layer Meteorology* **78**, 351–382.

Raupach, M. and Shaw, R. (1982) Averaging procedures for flow within vegetation canopies. *Boundary Layer Meteorology* **22**, 79–90.

Raupach, M. and Thom, A. (1981) Turbulence in and above plant canopies. *Annual Reviews of Fluid Mechanics* **13**, 97–129.

Shaw, R.H., Gao, W.G. and Paw U, K.T. (1989) Detection of temperature ramps and flow structures at a deciduous forest site. *Agricultural and Forest Meteorology* **47**, 123–138.

Shraiman, B.I. and Siggia, E.D. (2000) Scalar turbulence. *Nature* **405**, 639–646.

Siqueira, M. and Katul, G. (2002) Estimating heat sources and fluxes in thermally stratified canopy flows using higher-order closure models. *Boundary Layer Meteorology* **103**, 125–142.

Siqueira, M., Katul, G. and Lai, C.T. (2002) Quantifying net ecosystem exchange by multilevel ecophysiological and turbulent transport models. *Advances in Water Resources* **25**, 1357–1366.

Siqueira, M., Lai, C.T. and Katul, G. (2000) Estimating scalar sources, sinks, and fluxes in a forest canopy using Lagrangian, Eulerian, and Hybrid inverse models. *Journal of Geophysical Research* **105**, 29475–29488.

Siqueira, M., Leuning, R., Kolle, O. *et al.* (2003) Modelling sources and sinks of CO2, H2O and heat within a Siberian pine forest using three inverse methods. *Quarterly Journal of the Royal Meteorological Society* **129**, 1373–1393.

Siqueira, M.B. and Katul, G.G. (2010) An analytical model for the distribution of CO_2 sources and sinks, fluxes, and mean concentration within the roughness sub-layer. *Boundary-Layer Meteorology* **135**, 31–50.

Siqueira, M.B., Katul, G.G. and Tanny, J. (2012) The effect of the screen on the mass, momentum, and energy exchange rates of a uniform crop situated in an extensive screenhouse. *Boundary Layer Meteorology* **142**, 339–363.

Smits, A.J., McKeon, B.J. and Marusic, I. (2011) High Reynolds number wall turbulence. *Annual Review of Fluid Mechanics* **43**, 353–375.

Spano, D., Snyder, R.L., Duce, P. and Paw U, K.T. (2000) Estimating sensible and latent heat flux densities from grapevine canopies using surface renewal. *Agricultural and Forest Meteorology* **104**, 171–183.

Spano, D., Snyder, R.L., Duce, P. and Paw U, K.T. (1997) Surface renewal analysis for sensible heat flux density using structure functions. *Agricultural and Forest Meteorology* **86**, 259–271.

Sutton, M., Fowler, D. and Moncrieff, J. (1993) The exchange of atmospheric ammonia with vegetated surfaces. *Quarterly Journal of the Royal Meteorological Society* **119**, 1023–1045.

Thomas, C. and Foken, T. (2007) Flux contribution of coherent structures and its implication for the exchange of energy and matter in a tall spruce canopy. *Boundary Layer Meteorology* **123**, 317–337.

Thomas, M.D. (1951) Gas damage to plants. *Annual Review of Plant Physiology and Plant Molecular Biology* **2**, 293–322.

Tsallis, C. (1988) Possible generalization of Boltzmann–Gibbs statistics. *Journal of Statistical Physics* **52**, 479–487.

Warhaft, Z. (2000) Passive scalars in turbulent flows. *Annual Review of Fluid Mechanics* **32**, 203–240.

Wells, M., Clercx, H.J.H. and van Heijst, G. (2007) Vortices in oscillating spin-up. *Journal of Fluid Mechanics* **573**, 339.

Williams, C.G., LaDeau, S.L., Oren, R. and Katul, G.G. (2006) Modeling seed dispersal distances: Implications for transgenic *Pinus taeda*. *Ecological Applications* **16**, 117–124.

Wilson, N.R. and Shaw, R.H. (1977) A higher order closure model for canopy flow. *Journal of Applied Meteorology* **16**, 1198–1205.

Wolfe, G.M. and Thornton, J.A. (2011) The Chemistry of Atmosphere-Forest Exchange (CAFE) Model – Part 1: Model description and characterization. *Atmospheric Chemistry and Physics* **11**, 77–101.

Zhang, Y., Liu, H., Foken, T. *et al.* (2011) Coherent structures and flux contribution over an inhomogeneously irrigated cotton field. *Theoretical and Applied Climatology* **103**, 119–131. DOI: 10.1007/s00704-00010-00287-00706.